

To appear in the *Astronomical Journal*, March 2008

The Early Spectra of Eta Carinae 1892 to 1941 and the Onset of Its High Excitation Emission Spectrum

Roberta M. Humphreys, Kris Davidson and Michael Koppelman

Astronomy Department, University of Minnesota, 55455
roberta@umn.edu

ABSTRACT

The observed behavior of η Car from 1860 to 1940 has not been considered in most recent accounts, nor has it been explained in any quantitative model. We have used modern digital processing techniques to examine Harvard objective-prism spectra made from 1892 to 1941. Relatively high-excitation He I $\lambda 4471$ and [Fe III] $\lambda 4658$ emission, conspicuous today, were weak and perhaps absent throughout those years. Feast et al. noted this qualitative fact for other pre-1920 spectra, but we quantify it and extend it to a time only three years before Gaviola’s first observations of the high-excitation features. Evidently the supply of helium-ionizing photons ($\lambda < 504 \text{ \AA}$) grew rapidly between 1941 and 1944. *The apparent scarcity of such far-UV radiation before 1944 is difficult to explain in models that employ a hot massive secondary star*, because no feasible dense wind or obscuration by dust would have hidden the photoionization caused by the proposed companion during most of its orbital period. We also discuss the qualitative near-constancy of the spectrum from 1900 to 1940, and η Car’s photometric and spectroscopic transition between 1940 and 1953.

Subject headings: stars:individual(η Car) — stars: emission-line — stars:winds

1. Introduction

Eta Carinae is famous for its many superlatives as the most massive, most luminous star in our region of the Milky Way and for its “great eruption” (1837-1858) more than 160 yrs ago, when it ejected $6 M_{\odot}$ or more (Davidson & Humphreys 1997, Morris et al 1999, Smith et al 2003a) forming its bipolar Homunculus Nebula. η Car is also our closest and best studied example of a “supernova impostor”, but there are still numerous unsolved

questions about the cause of the great eruption and the star’s subsequent and on-going recovery. One of the most outstanding is its continuing instability and what happened when η Car experienced two post-eruption episodes of spectroscopic and photometric change: the second eruption (1888 - 1895) and again from about 1941 to 1952 when it rapidly brightened twice and the first mention of the high excitation emission lines appears in the astronomical literature (Gaviola 1953). The latter event has received little attention, although it may be fundamental to understanding the star’s process of recovery.

It is now well known that η Car experiences a spectroscopic/photometric 5.5 year cycle (Whitelock et al. 1994, Damineli 1996) . Modern groundbased spectra normally show high excitation emission lines, notably of He I, [Fe III], [Ne III], etc. sometimes referred to as the excitation maximum or “high state”. During a spectroscopic event or excitation minimum (low state) however, the high excitation lines weaken and even disappear. These “events” apparently last from a few weeks to a few months, and were noticed by several authors before 1996 (Gaviola 1953, Thackeray 1967, Rodgers & Searle 1967, Viotti 1968, Whitelock et al. 1983, Zanella et al. 1984, Bidelman et al. 1993). The 5.5 year spectroscopic cycle has been confirmed beginning with Gaviola’s (1953) first recorded evidence for a spectroscopic change in 1948 up to the most recent events in 1998.0 and 2003.5 (Damineli et al. 2000, Davidson et al. 2000, 2005).

Feast, Whitelock and Marang (2001) examined the spectra of η Car obtained at the Radcliffe Observatory in South Africa from 1947 to 1974 and confirmed the cycle as expected. However, they also reported that the earliest spectra from 1899 to 1919 never showed the high excitation state. Gaviola (1953) had also noted that the He I emission lines were not present in the spectra described by Moore and Sanford (1913, 1916) and Lunt (1919). The plates examined by Feast et al. (2001) included two from 1912-1914 described by Moore and Sanford plus an additional plate from 1914 and two others discussed by Lunt. Feast et al. also discussed Gill’s early spectrum (Gill 1899) and reexamined his measurements, but the plate could not be located. Thus they examined five plates in total which they said were “of excellent quality”, looking specifically for the He I line at 4471Å which should have been easily discernible.

Therefore from approximately 1899 to 1919 the star’s spectrum was never in the high excitation state, and there were no spectroscopic events as we understand them now. The 5.5 yr cycle has become an important part of η Car’s expected behavior, and has been variously attributed to 1) the presence of a hot secondary star which is eclipsed by η Car (Damineli et al. 2000) blocking the UV radiation for the high excitation lines, 2) a disturbance in the wind and mass ejection (Zanella et al. 1984, Davidson 1999, Davidson et al. 2000), or 3) a combination of the two (Davidson 2005). The absence of high excitation lines and the

spectroscopic cycle in these early spectra naturally raises questions about the origin of the cycle and when and why the high excitation lines first appeared.

The spectroscopic record from 1920 to the time of Gaviola’s spectral series beginning in 1944 was missing in the Feast et al. survey. However, the famous Harvard plate collection contains a series of objective prism plates of the Southern sky covering 1891 to 1951. We examined all of the available plates with spectra of η Car at the Harvard-Smithsonian Center for Astrophysics (CfA). In 2003 the staff at CfA had just begun a trial program to digitize the Harvard plate collection, and we were permitted to select several representative spectra for digitization.

In the next section, we describe the Harvard spectra of η Car obtained from 1892 to 1941, and our rectification, calibration and extraction process. In §3 and §4, respectively, we discuss the earliest spectra from the time of the second eruption, and those from 1902 to 1941. Measurements of the digitized spectra and comparison with recent groundbased spectra show that *He I λ 4471 emission was absent or only marginally present*. If present at all, it was *much weaker* than reported by Gaviola and insignificant compared with current spectra. Similarly, the [Fe III] lines in these spectra are either absent or marginal, and there were apparently no spectroscopic events. This result has serious implications for the origin of the He I and the high excitation lines in η Car discussed in the rest of this paper. In §5 we describe the the apparent changes in η Car’s wind over more than 50 yrs and the onset of the high excitation emission during the period of rapid photometric change from \sim 1941 to 1952. We review the He I emission problem in §6 including the possible sources of present day He I emission in η Car and its absence prior to 1944. Our conclusions are summarized in the last section.

2. The Harvard Objective Prism Spectra

The Harvard plate collection includes spectra of η Car in three different series of objective prism plates, listed in Table 1. The most extensive and most useful is the *X* series obtained with a single prism on the 13-inch Boyden refractor. Spectra of η Car were obtained with this telescope in 1892 – 1926 and 1937 – 1941. The telescope was moved from Arequipa, Peru to Bloemfontein, South Africa in 1930 where it was used until 1951. These spectra thus form a fairly uniform set obtained with the same instrument over nearly 50 yrs., although it is unfortunate that η Car was not observed after 1941 when the star underwent a major photometric and spectroscopic change.

We examined all of the *X* series plates that included spectra of η Car plus a few very

early spectra in the *A* and *B* series. These plates are listed in the Appendix (Table A1) in chronological order with notes on the spectra. Figure 1 shows the dates of the spectra superposed on a partial light curve of η Car together with the times of the early spectra from the Radcliffe Observatory (Feast et al. 2001) and Gaviola’s spectra (Gaviola 1953). Figure 2 shows their distribution with phase in the 5.5 yr spectroscopic cycle.

The highest quality spectra and the best of those representative of different times or phases in the spectroscopic cycle were selected for digitization at CfA and are identified in Table A1. They were digitized with a Umax Power Look 3000 scanner with 1200 bpi and a 14 bit grayscale. Figure 3 shows one example, an unusually long exposure that clearly shows other stars around η Car. The plate scale was 42 arcsec/mm while the spectral dispersion was about 28 Å/mm at $\lambda = 4000$ Å and 64 Å/mm at 5000 Å. The separation between 4000 and 5000 Å was about 24 mm, equivalent to an angular distance of almost 17′. The digitized pixel values represent photographic densities, which would be very difficult to calibrate since there were complicated variations in exposure times, photographic response, etc. The analysis in this paper, however, does not depend on quantitative relations between pixel values and radiation flux.

Many of the objective prism spectra have non-uniform guiding. The earliest spectra are skewed on the plate, and many of the later spectra have an obvious curvature (Figure 3). Correcting for these problems and converting each spectrogram to a one-dimensional spectrum was a non-trivial exercise. We first rotated the image so that η Car’s spectrum extended accurately along image rows. As Fig. 4a shows, the resulting spectrogram, consisting of several dozen digitized image rows, was typically distorted by non-uniform guiding. Careful analysis of the emission lines showed small-scale irregularities – e.g., abrupt changes in tracking rate or direction – that are not all obvious to the eye. Using an iterative cross-correlation technique to find the best horizontal offset for each image row, we straightened the spectrum as shown in Figs. 4b and 4c. We discarded wavelengths outside the range 3700–5300 Å. Finally, we combined the rows by the following procedure which eliminated most scratches and localized defects: (1) Each digitized pixel value was divided by the average value along its row. (2) Then, in each column we rejected high and low values, typically those outside the 15th and 85th percentile. (3) Finally we took a weighted average of the remaining pixels in the column, where each weight was based on the average value along that pixel’s row. In principle the non-linear photographic response makes some of these steps questionable; but in practice they worked quite well. Most scratches and spots on the plates – even some alarmingly conspicuous ones – had almost no effect on the resulting one-dimensional spectra, and the exceptions were easy to identify. Our procedure also reduced the effects of instances where unsteady tracking caused a row to be seriously over or

underexposed, or where the telescope accidentally lurched along the dispersion direction ¹.

An accurate wavelength calibration was necessary for judging the presence or absence of He I $\lambda 4471$, discussed later. The only feasible calibration data were emission lines in the spectrum of η Car itself. Practically all of these were unresolved blends, usually of Fe II and [Fe II] lines which originate at various distances from the star; and in principle the line ratios within each blend depend on the spatial coverage and evolve with time as the ejecta densities progressively decrease. Therefore, as reference standards we used wavelengths measured by Gaviola from spectra obtained in the 1940’s. His were the earliest and most complete published data with sufficient accuracy and were obtained relatively close to the time to when many of the objective prism plates were observed. His data were photographic, and the spectra were “slitless”, with a comparison spectrum exposed before and after through a superimposed slit. Like the objective prism spectra, they include the entire star plus nebula. In each of the selected spectrograms we measured 12 to 22 emission features (blends) in the wavelength range 4173–5018 Å, not using any hydrogen lines or blends that might include helium emission. Then we fit the measurements to a “Hartmann formula,”

$$x = a + \frac{b}{(\lambda - c)},$$

where we determined the adjustable parameters a , b , and c separately for each individual case. This expression resembles the prism dispersion much better than a three-parameter polynomial does, and we found that a fourth parameter did not materially improve the fit. In a simple model the wavelength asymptote c should have been a constant for all the plates; in fact the best-fit values were all in the range 1930–2070 Å, acceptably similar, under the circumstances.

The resulting wavelength calibrations were remarkably good. The r.m.s. deviation of individual data points from the three-parameter fit was typically ± 0.25 Å, and about ± 0.15 Å for the best spectrogram, X16614. The *formal* one-sigma uncertainty in the wavelength fit around 4500 Å was therefore only about ± 0.1 Å (7 km s^{−1}) for most cases and ± 0.04 Å for X16614. To some extent *systematic* effects are constrained by a test noted below. On the other hand, since 12–22 points were used to adjust a three-parameter formula with an appropriate functional form, the calibration errors for wavelength *differences* between features in any 100-Å interval near the middle of the range are presumably much smaller than 0.1 Å.

¹FITS images of the digitized spectra and examples of the rectified spectra plus the wavelength calibrated tracings are available at <http://etacar.umn.edu/download/EarlySp> and with the electronic edition of the Astronomical Journal.

To forestall ambiguities in wavelength values quoted later in this paper, we shifted each spectrum to the laboratory wavelength system “in air” (STP). We assumed a Doppler velocity of -30 km s^{-1} , based on the measurements for the metallic emission lines by the early observers (Gaviola 1953, Lunt 1919). (*Caveat:* In η Car the hydrogen lines can have significantly different Doppler shifts than Fe II, [Fe II], Ni II, etc.)

The overall wavelength measurement errors are crucial to the discussion in Section 4 below. In order to assess the likely uncertainty, we measured the wavelength of [Fe II] $\lambda 4287.40$ in 12 spectrograms, using the same procedures as we did for the lines discussed in Section 4. This is the only strong feature that is dominated by a single, narrow, well-identified spectral line in these data, so (unlike the blends) there is no doubt about its correct laboratory wavelength. Since we did not give it extra weight in the wavelength calibration, it is a valid reference for testing our measurement technique. We measured the near-peak part of the line, essentially the centroid wavelength in the upper 20% of the feature’s net height; this quantity is well-suited to the non-linear photographic response. Among the 12 spectra, the r.m.s. deviation from 4287.40 \AA was $\pm 0.22 \text{ \AA}$. Several of them, however, were recognizably of low quality, with asymmetric or blurred emission features. When we omitted three obviously poor spectra, the r.m.s. wavelength error improved to $\pm 0.13 \text{ \AA}$.

This estimate is smaller than the r.m.s. data-point deviation quoted above for the wavelength calibration – which is not very surprising, since wavelengths *assumed* for that procedure were inexact, representing blends rather than individual spectral lines. (Errors in the assumed wavelengths of blends presumably averaged out in the calibration process, since many independent blends were used as data points.) Thus, in the absence of additional information, $\pm 0.13 \text{ \AA}$ is the best error estimate we can make for a careful measurement in a satisfactory spectrogram. We emphasize one major exception, however: *spectrum X16614 was conspicuously better*. It had much sharper features than most of the others (See Fig. 11), and produced formally better wavelength-calibration statistics. Its exposure level, guiding, etc. must have been fortuitously optimal. Judging from all the considerations outlined above, the standard error for a wavelength measurement in X16614 is $\pm 0.1 \text{ \AA}$ or better; informally we suspect that $\pm 0.08 \text{ \AA}$ would be a realistic estimate for well-defined spectral features in X16614. We measured 4287.34 \AA for the [Fe II] $\lambda 4287.40$ line in X16614.

3. The Earliest Spectra 1892 – 1898

The first spectrum of η Car was a visual observation by Le Sueur (1870) who described strong emission lines, and the first photographic spectrogram was obtained on May 15, 1892 with the Harvard 13-inch Boyden telescope at Arequipa. The spectrogram from June 2 1893,

X4709, is of especially good quality and has been described by several authors including Cannon (1901), Bok (1930), Hoffleit (1933), Whitney (1952) and most recently by Walborn and Liller (1977). Unlike spectra observed after 1895, it shows a well developed absorption line spectrum resembling an F-type supergiant plus strong emission lines of hydrogen, Fe II and [Fe II]. These earliest Harvard spectra from 1892 to 1895 were obtained when η Car was in its second or lesser eruption (1888 – 1895). The F-type supergiant spectrum, combined with the star’s apparent brightening of about two magnitudes which lasted ~ 7 yrs, suggests that this was a classic LBV or S Doradus-type eruption with an optically thick cool wind (Humphreys, Davidson & Smith 1999, Humphreys & Davidson 1994).

Our digitized scan of the famous 1893 spectrogram is shown in Figure 5 with the rectified scan, and the extracted tracing. A good reproduction of the original photographic spectrum can be seen in Walborn and Liller (1977). The procedure described above (§2) for the wavelength calibration was unsuitable for X4709 because its spectrum was fundamentally different. Instead, we used several emission lines measured by Whitney (1952), who used a difficult calibration procedure based on the hydrogen lines in the spectra of other stars on the plate. Thus our wavelength calibration for X4709 is not as good as the cases described above. Whitney gave a comprehensive list of numerous identified absorption lines with estimated line intensities that are consistent with its early-to-mid-F-type supergiant classification. His measured velocity of -180 km s^{-1} for the absorption lines relative to the H emission lines is indicative of an expanding envelope consistent with the comparatively slow winds in LBV eruptions (Humphreys & Davidson 1994). Weak absorption features, attributed by Whitney to hydrogen absorption, can be seen to the blue of the $H\gamma$ and $H\delta$ emission lines and may be due to P Cygni absorption. Using our wavelength scale, we measured velocities at the base of the absorption, relative to the hydrogen emission peaks, of -300 km s^{-1} , significantly slower than η Car’s current polar wind (Davidson & Humphreys 1997, Smith et al. 2003b), but comparable to the polar expansion velocity in the “little homunculus” (Smith 2005) from material probably ejected in the second eruption.

The additional spectrograms obtained between 1892 and 1900 are described in Table A1, although most of the spectra from this period are too weak to confidently identify the lines. We note that the F-type absorption lines had vanished by 1895 when the second eruption had ended. Spectra at lower dispersion from 1897 and 1898 show only hydrogen emission. Beginning with the observations in 1902, the spectra begin to show the prominent emission line spectrum of hydrogen, [Fe II], and Fe II that is familiar in all subsequent groundbased spectra of η Car.

4. The Spectra from 1902 to 1941

The Harvard spectra have good coverage during several intervals: 1902–1904, 1913–1916, 1922–1926, and 1937–1941. The best spectrogram, X16614 obtained on 29 March 1938, is shown in Figure 6. Figures 7 and 8 show expanded regions of the same spectrum with some of the stronger lines identified.

For reasons given in the Introduction and discussed in §5 and §6, it is important to determine whether helium emission features were present. In the wavelength range covered by these spectra, the most suitable and strongest line is He I $\lambda 4471.5$ which was also discussed by Feast et al (2001). Figure 9 shows an obvious emission feature or blend centered at 4473.7\AA in X16614, with an expected measurement uncertainty of better than $\pm 0.1\text{\AA}$ ². This wavelength refers to both the peak and the centroid of the brightest part of the feature. Four emission lines are expected between 4470\AA and 4475\AA (Aller & Dunham 1966). Apart from helium $\lambda 4471.5$, the feature is dominated by [Fe II] $\lambda 4474.9$ plus two weaker lines, Fe II $\lambda 4472.9$ and [Fe II] $\lambda 4470.3$. Gaviola (1953) states that He I $\lambda 4471.5$ was about the same strength as [Fe II] $\lambda 4474.9$ when his spectra were obtained in 1944–1951. If this feature were a simple blend of these two lines, its expected central wavelength would be 4473.2\AA , significantly to the blue of the feature in X16614. Based on Gaviola’s eye estimates, the Fe II $\lambda 4472.9$ line was much weaker than the $\lambda 4474.9$ line, and the $\lambda 4470.3$ line was blended with He I in his spectra. Thus the 4473.7\AA emission feature in X16614 is obviously a blend, and He I $\lambda 4471$ was apparently weaker than in Gaviola’s spectra after 1944. Whether or not it was present in X16614 depends on the relative strengths of the other three lines.

For reasons noted later, our quantitative assessment of the pre-1941 high-excitation features will rely on comparisons with published spectra obtained in 1944–1961, and not on the spectrum seen today. Nevertheless, in Figures 9 and 10, we show X16614 together with recent groundbased data, because they clearly show the pertinent features and they are readily available while tracings of older spectrograms are not. These modern data were obtained using the GMOS-S on the Gemini South telescope on 2007 June 11, with exposure time 5 s, slit width $0''.5$, and seeing about $1''.5$. The tracings in Figs. 9 and 10 represent an extraction width of $1''.5$ along the slit. Because of the unusually poor seeing, in effect the extracted spectrum samples a region almost $2''$ across, including about 60% of the total brightness of the star plus Homunculus Nebula (see Figs. 2 and 3 in Martin et al. 2006b). It therefore shows the broad-line spectrum of the opaque stellar wind combined with narrower

²Using a simple interpolation between [Fe II] 4458\AA and the Fe II blend at 4490\AA , Humphreys and Koppelman (2005) originally estimated a line center of 4474.0\AA .

lines from slow-moving material ejected many years ago.³ The vertical scale is linear for the Gemini tracing and quasi-logarithmic for X16614, but here we are chiefly interested in wavelengths rather than flux values. The wavelength scale is in the laboratory rest system for both spectra. Note that the wavelength correspondence between the 1938 and 2007 spectra is quite good.

The He I and [Fe II] 4474.9Å lines are easily separated in the recent Gemini spectrum. The peak or center of the objective prism 4473.7Å emission feature is in the trough between these two lines, but shifted appreciably to the red with respect to the weighted centroid (at 4472.9Å) of the two present day emission peaks. If He I were present in the objective prism spectrum in comparable strength to the current spectrum, it would appear as a bump or shoulder on the blue side of the 4473Å feature. If it were present in approximately equal strength to [Fe II] 4474.9Å, as Gaviola reported, then the peak or center of the blend would be at about 4473.2Å, as we noted above. The Fe II 4472.9Å line can just barely be discerned in the Gemini spectrum as a small bump on the red side of the He I profile which we measured at 4473.1Å. Although it is one of the weaker lines in Fe II multiplet 37, we believe this identification is correct, because all of the stronger lines and one weaker line in multiplet 37 are all present in the recent spectrum. We also identified all of the same lines in the 1938 spectrum. This Fe II line was thus present then and contributed to the observed 4473.7Å profile in X16614.

Today a substantial fraction of η Car’s observed light comes directly from the emitting regions, and the star can be separated from its slow-moving inner eruptive ejecta at high spatial resolution; see Martin et al. (2006b) and refs. therein. Several decades ago, however, the situation was qualitatively different. Circumstellar extinction was then so large that nearly all of the observed visual-wavelength light escaped *only after being scattered by slow-moving dust grains* (see Davidson and Ruiz 1975 for a typical model). Then as now, the inner radius of the dusty region should have been 150 to 600 AU, depending on grain details; but optical depths were then larger than today’s, and more slow-moving ejecta were located fairly close to the star. Thus, before about 1970 or 1980, most spectrograms of η Car represented a mixture of broad emission features from the stellar wind plus narrow lines from inner slow-moving ejecta, altogether diffusing out through a scattering nebula. Only about 10% of the light escaped. The scattering region had an apparent diameter of the order of 2'', and contained a central dust-free zone because grains could not exist close to the central star. In view of these circumstances, we shall use pre-1970 spectrograms, not modern data,

³ HST/STIS data contain more detail and they do not mix the spectra of η Car’s wind and nearby slow ejecta together as ground-based observations do. See archives at <http://etacar.umn.edu/> and <http://archive.stsci.edu/prepds/etacar>.

as reference comparisons for the old objective prism spectra. The most useful examples are Gaviola (1953), because most of his spectra were obtained before 1950; and Aller and Dunham (1966), because they carefully calibrated the relative line intensities visible in 1961.

Our analysis depends on wavelengths. In order to avoid possible misunderstandings, let us make some preliminary comments about Doppler shifts. First, there is no reason to think that Doppler shifts caused by scattering would especially perturb the high-excitation He I and Fe III lines; no such effect can be seen in the measurements reported by Gaviola and by Aller and Dunham, and in general one expects the entire spectrum produced near the star, both low- and high-excitation lines, to be similarly affected by the scattering process. In a related connection, we note that Doppler shifts of more than 100 km s^{-1} occur when the central spectrum is reflected by fast outward-moving material in the Homunculus lobes (Davidson et al. 2001 and older refs. therein). This fact has no effect on our measurements, because the Homunculus lobes were relatively faint; the objective prism plates, Gaviola’s spectrograms, and that of Aller and Dunham were all strongly dominated by the bright central core mentioned above. This can be seen in those authors’ measurements and in the tracings shown by Aller and Dunham, which resemble the modern Gemini spectra to a surprising degree. Their Fig. 2 is especially relevant because it shows the He I $\lambda 4471.5$ line. Next, the present-day *broad* He I $\lambda 4471.5$ profile fluctuates throughout η Car’s 5.5-year spectroscopic cycle; its centroid wavelength is generally a little smaller than 4471.5 \AA , which should make the feature more, not less, evident in the type of analysis we employ below. Since we find a non-detection, we do not attempt to correct for this complex effect. Finally, we note that most pre-1970 spectrograms of η Car did not perceptibly depend on their chosen slit sizes or even the absence of a slit. They were dominated by the bright central core, and atmospheric seeing caused nearly the entire core to be sampled within any normally-used slit width.⁴

To determine whether He I emission was present in the 1938 spectrum we must estimate the relative strengths of the [Fe II], Fe II and He I lines required to produce the observed blended profile. A detailed model of the profile would require quantitative information about the photographic response which is no longer available. Instead, we have adopted the spectrophotometric measurements of the line strengths from Aller & Dunham’s (1966) high resolution Coudé spectra from 1961. Using their values we find an average wavelength of 4473.7 \AA for the [Fe II], Fe II blend, i.e., not including any He I $\lambda 4471.5$ emission. *Thus no contribution from He I $\lambda 4471.5$ is required to produce the observed line center at 4473.7 .* X16614 was obtained at phase 0.22 in the present-day 5.5 yr cycle, so it does not correspond

⁴ The only exceptions to this statement were slit spectra of the outer Homunculus that avoided the central object; but they are irrelevant in this paper.

to a spectroscopic event. Aller & Dunham’s spectra were obtained more than 20 yrs after X16614, so as a check, we also used Gaviola’s eye estimates of the line strengths and obtained the same result.

The expected one sigma error for this measurement in X16614 is less than 0.1\AA (§2). Thus allowing for an overall uncertainty of $\pm 2\sigma$, the line center is between 4473.5 and 4473.9\AA . Any shift to the red would confirm no contribution from He I. If we adopt a line center at 4473.5\AA as the shortest feasible wavelength, the He I contribution is still small, less than 10% of the total blend and about 18% as bright as the $\lambda 4474.9$ line observed in 1961. In that case, He I in 1938 would have been less than one-fourth its strength seen in Gaviola’s 1944-51 spectra when He I and [Fe II] $\lambda 4474.9$ were about equal. Based on other line ratios in both the 2007 Gemini data and Aller & Dunham’s 1961 spectrum, it is fair to conclude that $I(\text{He I } \lambda 4471) < 0.003I(\text{H}\beta)$ in 1938. *Thus we conclude that helium emission was quite weak and may have been virtually absent in 1938.*

None of the other strong high excitation lines visible in modern spectra are apparent in the 1938 spectrum ⁵. The best example is [Fe III] emission at $\lambda 4658.1$ which is quite strong in the spectra of eta Car described since 1951 (Thackeray 1953, Aller & Dunham 1966, Zethson et al 1999). The [Fe III] emission lines are present in Gaviola’s data, but notably weaker than in later spectra. If [Fe III] $\lambda 4658$ is present in X16614, it is part of a broad complex emission profile from 4652\AA to 4674\AA due to several different lines (Figure 10). The red peak in this profile at $\lambda 4666.7$ is due primarily to Fe II $\lambda 4666.75$, and the profile also includes Fe [II] $\lambda 4663.7$, [Fe II] $\lambda 4664.5$ and Fe II $\lambda 4670.2$. We measure a center for the much smaller secondary peak on the blue side at 4657.5\AA . In addition to a possible contribution from the [Fe III] line, Fe II $\lambda 4657.0$ and [Co II] $\lambda 4657.4$ (Zethson 2001) plus lines of Cr II are also present. Given the complexity of this profile, and the lack of a recognizable peak due to the [Fe III] line, visible in the later spectra, it is difficult to ascertain if it is present, although a weak feature just above the continuum at 4701.1\AA may be [Fe III] $\lambda 4701.5$. Assuming that some [Fe III] emission is contributing to these features, then like He I, they are much weaker, with respect to other emission lines, than in the later spectra. In the course of comparing the objective prism spectra with Gaviola’s spectra and other published line lists and intensity estimates in the literature, we noticed that beginning in 1951-52 the apparent strength of the high excitation emission lines appeared to increase compared to the Fe II and [Fe II] spectrum. To document this we compared the line ratios of He I $\lambda 4471.5\text{\AA}$ relative to [Fe II]

⁵A weak emission feature is present at $\lambda 4713.9$, but given its measured wavelength and the absence of any other He I lines in the spectrum, we concluded that this is not He I $\lambda 4713.1$, but more likely a blend of Fe II and Cr II. If it were He I $\lambda 4713$, with normal helium line ratios, then we should have easily detected $\lambda 4471$.

4474.9Å and [Fe III] 4658Å to [Fe II] 4639.7Å from several sources using their own estimates of the line strength or intensities. These are summarized in Table 2. The He I emission has remained relatively constant since ~ 1951 , while the strength of [Fe III] has gradually increased. Decreasing gas densities may partially explain this trend.

We adopted the 1938 spectrum as a template or reference for comparison with all of the other digitized spectra from 1902 to 1941. We looked for any changes in the profile and central wavelength of the 4473.7Å emission feature as well as any other obvious changes in the spectrum. This emission feature is present in all of the spectra independent of phase in the 5.5 yr cycle. In the earliest spectra (1902 - 1916), this line was noticeably much weaker than in the 1938 spectrum and barely visible above the noise in some cases (Figure 11). This is obviously the line noted by Feast et al (2001) and seen by the early observers in spectra from 1913 and 1919. We therefore concur with Feast et al that He I was not present in any significance in these spectra and that the observed feature is a blend of the Fe II and [Fe II] lines. The [Fe III] emission lines are not present in any of these earliest spectra. In the spectra from 1922 to 1941, the 4473.7Å emission feature is virtually identical to the same feature in the 1938 reference spectrum with respect to the shape of the profile and the measured central wavelength of the blend. We also note that the [Fe III] lines at 4658Å and 4701Å are either absent in most of these spectra or, may be marginally present in a few, as in X16614. The related [Ne III] emission lines (Zanella et al. 1984) are outside the wavelength range where these plates were sensitive.

Did spectroscopic events occur before 1948? Only a few of the Harvard spectra were obtained near the time of an expected “event” (Fig. 2). Those from May 1937, phase 0.06, show no apparent change in the spectrum or in the 4473.7Å emission feature. Evidently, between the time of the last spectrum in the Harvard series from May 1941 and Gaviola’s spectral series beginning three years later in 1944, the high excitation lines appeared and the He I emission increased significantly in relative intensity. The star also brightened by almost a magnitude sometime between 1939 and June 1941 (O’Connell (1956), de Vaucouleurs & Eggen (1952)). η Car’s wind was apparently in a critical transition during that time. For this reason we carefully inspected the spectra between 1938 and 1941 for any spectroscopic evidence and found no obvious change.

Viewing all the Harvard plates together, one especially notices how similar all of these spectra appear after 1900. They all show the same qualitatively similar features. Moreover, apart from He I and the strong high-excitation lines, they closely resemble subsequent low-resolution groundbased spectra since 1950. This is remarkable because the Homunculus nebula tripled in size during the twentieth century, and the object experienced more than one episode of rapid brightening.

In summary we conclude that *the helium emission lines were quite weak, practically absent, during the period 1902–1941*. This applies to both the broad and narrow components. Similarly, the high excitation forbidden lines were either absent or very weak. η Car’s spectrum was thus always in the “low excitation state” from 1900 to 1941. This fact has serious implications discussed in §5 and §6 below.

5. Variations in the Wind of Eta Car 1870 to 1951

Beginning with the first visual spectroscopic observation by Le Sueur (1870), we can recognize four different stages defined by the appearance of η Car’s spectrum and its light curve; (1) post-eruption 1858 - 1887, (2) the second eruption 1888 - 1895, (3) quiescence \sim 1900 - 1941, and (4) the spectroscopic/photometric transition 1941 - 1952.

5.1. Post-Eruption

We know very little about the physical state of the star after the great eruption except that it faded rapidly after 1857. This is usually attributed to the formation of dust which probably occurred quickly after the cessation of the eruption, although the exact time when the eruption ended is not clear from the light curve. Le Sueur’s (1870) visual observation about 10 years later is especially intriguing. He described five emission lines, the Fraunhofer lines C ($H\alpha$), D, “b group” and F ($H\beta$) plus the “principal green nitrogen line”. The Fraunhofer b group, due to Mg I absorption in the Sun (5167 – 5184Å), is very likely [Fe II] 5158Å and Fe II 5169Å emission in η Car. The “D” line is especially interesting, because although Na I D is present today in η Car as a complex mix of absorption and emission, it is not a strong emission line. Strong Na D emission occurs in much cooler stars. Le Sueur says the yellow or orange line is “very near D”. Thus it is possible that it was actually He I 5876Å and if so it had to be at least as strong then as it is now. In current groundbased spectra it is comparable in strength to the [N II] 5755Å line which apparently wasn’t noticed by Le Sueur. It is clear from the text that this was a difficult observation, near the limit of what could be seen, so it is possible that He I 5876Å and other emission lines were much stronger then. As this was only about 10 years after the great eruption during which η Car had thrown off its entire outer envelope, we can only speculate about the origin of a He I line, but it could either originate in a hot wind or even from what was then its photosphere. Walborn and Liller (1977) earlier made these same identifications based on Le Sueur’s description and suggested that the green nitrogen line was [Fe II] λ 5018 because of Le Sueur’s statement that it was not just an extension of the nebular emission line, presumably [O III] λ 5007, across

the spectrum of η Car ⁶ .

5.2. The Second Eruption

The second or lesser eruption is now best understood as similar to a classical LBV or S Doradus-type eruption or optically thick wind stage (Humphreys et al 1999) during which the expanded wind or “pseudo-photosphere” is relatively slow, dense, and cool with an enhanced mass loss rate. The second eruption was not as minor as it may appear on the historical light curve (Figure 1). When corrected for a realistic estimate of the circumstellar extinction at that time, the star’s apparent brightness would have been about second magnitude (Figure 3 in Humphreys et al. 1999), and its expanded, cool envelope with its F supergiant spectrum would have reached $r \sim 6$ AU. The star also ejected about $0.2 M_{\odot}$ of slow moving material in both the equatorial and the polar directions (Davidson et al. 2001, Ishibashi et al 2003, Smith 2005). Thus in both the great and second eruptions, η Car ejected mass with a bipolar structure. The cause of this second outburst is not known, but the most likely explanations for LBV-type eruptions include the opacity modified Eddington limit, subphotospheric gravity-mode instabilities, and a super-Eddington continuum -driven wind (See reviews by Humphreys & Davidson 1994, Glatzel 2005, Owocki 2005, Shaviv 2005).

5.3. Quiescence \sim 1900 to 1941

The period from about 1900 to 1941 was one of relative quiescence for η Car. Its apparent brightness was basically constant at \sim 8th magnitude, and as we have described, the spectra from this period are remarkably similar. Weak He I emission may have contributed to the blended emission feature at 4473.7\AA but, if so, it was only marginally present and much weaker than observed after 1944. With very weak or absent He I and other high excitation lines, the spectrum was always in what is now called the low excitation state and there were no spectroscopic events.

Today we make a clear distinction between emission lines produced in η Car’s wind ($r < 15$ mas) and the features that originate in ejecta from past outbursts ($r > 0''.1$); see below. Groundbased spectra include both types together. Before 1950, however, this

⁶On the other hand, Schuster (1872) explicitly stated that “the green line” was near 5164\AA in an arc spectrum of nitrogen; perhaps he meant N II multiplets 35 and 37. This would coincide with Fraunhofer b, but Le Sueur did not explicitly say that he could distinguish “the principle green nitrogen line” from Fraunhofer b. Therefore, although Walborn and Liller’s suggestion still seems most likely, it is not certain.

distinction would have been less clear even if high spatial resolution had been available. The innermost dense ejecta were then closer to the star, and the wind may have been denser. The observed emission therefore must have escaped from the inner region via multiple scattering by dust grains (Davidson & Ruiz 1975). All emission sources within $1''$ of the star were thus mixed together in the emergent spectrum, as we noted in §4.

The broad He I emission lines originate in η Car’s wind as discussed in §6 below, while the narrow He I and high excitation forbidden lines are now known to come from slow moving diffuse gas near the star, including the Weigelt knots within $0''.3$ (Davidson et al 1995). The relevant high-excitation gas is presumably photoionized (Zanella et al. 1984; Davidson 1999). In the colliding-wind/X-ray eclipse model (Pittard & Corcoran 2002) for the spectroscopic events, the responsible UV radiation is assumed to come from the secondary star which is then eclipsed by the primary during an “event”. Despite a claim to the contrary (Iping et al. 2005), there is no unambiguous spectroscopic evidence for the companion (Hillier et al. 2001, 2006, Martin et al. 2006a). Various observational constraints, such as the 3000 km s^{-1} wind required for the X-ray spectrum and the star’s lack of visibility in the spectrum, suggest that the secondary must be a hot, main sequence star, much less luminous than η Car, probably an O-type star with initial mass of $\approx 40 - 60 M_{\odot}$ (Ishibashi 2001, Davidson 2005). It is thus a massive star, with a normal hot star wind, but far less massive than the primary.

But if this same star is the source of the UV radiation for the high excitation lines, there must be some explanation for why they were not observed for 40 years or more. Two possible explanations are obscuration of the secondary by either dust or by an optically thick wind from the primary, preventing the UV radiation from reaching the inner ejecta. There are feasible ways to prevent the *narrow* high excitation lines from originating 200–1000 AU from the central star; but the broad He I $\lambda 4471.5$ line formed in the wind is much harder to suppress. The UV flux from one or both stars will destroy dust within 100 AU and the expected dust formation distance is 150–600 AU. The semi-major axis of the secondary’s highly eccentric orbit is 17 AU so it is always well within the dust envelope. Therefore dust could not prevent its UV flux from ionizing helium in the primary’s wind, and we should have detected moderately broad He I $\lambda 4471.5$ emission (see Fig. 2 in Aller and Dunham 1966).⁷ The Weigelt knots, for example, are today $\approx 400 - 500$ AU from the star, but in

⁷ As D.J. Hillier (priv. comm.) remarks, conceivably one might devise an explanation based on inhomogeneities in the dust distribution. Observations since 1980 suggest that the star is behind a local extinction maximum with a size scale of only $0.2''$ (Davidson et al. 1995; Hillier & Allen 1992; Davidson & Humphreys 1986). If for this reason the pre-1941 spectrum mainly represented emission far from the star, then perhaps He I emission formed in the primary wind would have been hidden. An explanation of this type has several

1900 - 1940 this slow moving material, probably ejected in the 1890's eruption (Smith & Gehrz 1998), was also mostly inside the dust formation zone. Thus obscuration by dust cannot easily explain the weak or absent He I and high excitation lines prior to 1944. An optically thick wind that would enshroud the secondary throughout its orbit would also not suppress the broad He I lines, see §6.

5.4. The Spectroscopic/Photometric Transition 1941 - 1952

Between the end of 1939 and mid 1941 η Car brightened about 0.8 mag on the photographic scale (O'Connell 1956). Only three years later, the star's spectrum showed prominent He I emission and other high excitation emission lines. It continued to brighten for several years with small oscillations reaching 6.9 to 7.1 photographic by 1952 when de Vaucouleurs & Eggen (1952) reported a rapid increase from 6.9 to 6.5 mag in apparent visual brightness, measured photoelectrically, in only a few weeks from February to March 1952. It is important to realize that these measurements and eye estimates refer to the integrated light of the entire Homunculus not just to the central object. Neither of these brightenings correspond with a spectroscopic event; the preceding events occurred in 1937.0 and 1948.1⁸. The object's rapid brightening during this time was most likely due to dust destruction which might also be caused by the increase in UV radiation required for the onset of the He I and high excitation emission lines. As mentioned in §4, spectra obtained after 1951-52, show an increase in the strength of the high excitation emission lines such as [Fe III] compared to Gaviola's spectra. After 1952, the integrated light of the Homunculus continued to brighten slowly at a fairly regular rate, attributed to the expansion of the dust envelope, until HST/STIS spectra in 1998-99 revealed another rapid brightening, this time of the central star, of ~ 1 magnitude in only one year (Davidson et al 1999). Since then the integrated light has continued to brighten more rapidly than the previous long-term trend (Martin & Koppelman 2004, Martin et al. 2006b)

The colliding-wind binary model provides a reasonable working hypothesis for the X-ray light curve and the 5.5 yr period. However, main sequence hot stars with their radiatively driven fast winds are not expected to experience sudden increases in UV radiation implying a

difficulties, though. The $H\beta$ line in the objective prism spectra is perceptibly broad, indicating that it was formed in the wind; how can line-of-sight dust hide He I $\lambda 4471.5$ but not $H\beta$? Moreover, one would also need to explain why the high-excitation lines *did* appear in Gaviola's spectrograms in the mid-1940's.

⁸There are two gaps in the photometric record during the 20th century, 1915 - 1935 and 1953 - 1970. We suspect that a brightening of one magnitude or more would have been noticed especially in the 1950-60's when Thackeray was observing η Car frequently

drastic change in the wind and mass loss rate or an increase in the star’s surface temperature. Smith et al (2003b) proposed an explanation for the increase in the UV flux from η Car itself, the primary rather than its less massive companion, related to η Car’s recovery from its great eruption.

Smith et al. (2003b) and van Boekel et al. (2003) showed that the wind of η Car today is latitude dependent with a stronger, faster wind at the poles and a higher ionization and lower density wind in the equatorial region. Smith et al. suggest that more than a century ago, due its loss of several solar masses in the great eruption, the *surface* of η Car was rotating slowly within a dense spherical wind. The interior, with most of the mass, would have had the same higher specific angular momentum as before the great eruption. Thus the surface gradually spun up until its rotation rate was sufficient to form the present aspherical wind. This transition can be quite rapid, and the delay time of ~ 100 yrs is reasonable, so it may correspond to the rapid brightening in the early 1940’s and the onset of the high excitation emission due to UV photons which may now escape from the lower density equatorial zone. (See Davidson (2005) for some of the theoretical considerations.) In Smith et al.’s suggestion the spectroscopic events are due to equatorial ejections very likely triggered by the approach of the secondary at periastron (3 – 4 AU) to the massive primary which is already close to the Eddington limit. The increased density in the equatorial region due to even a small mass loss of order of $10^{-3}M_{\odot}$ would be sufficient to temporarily block the UV radiation. We note that HST/STIS observations of the two most recent spectroscopic events (1998.0 and 2003.5) show that they were not identical and confirm that η Car does indeed eject a shell (Davidson et al 2005, Martin et al 2006a). Furthermore, comparison of the STIS and UVES data (Stahl et al 2005) from the 2003.5 event show that it was latitude dependent. Changes in the wind at the higher latitudes were less dramatic, the wind became denser at the lower latitudes, and consequently, the spectra from the equatorial and polar regions were more alike during the spectroscopic minimum, consistent with the expectations from an equatorial shell ejection. The longer-term observational record also shows that these spectroscopic events are not identical either in their duration or their spectroscopic characteristics (See Humphreys 1999, Feast et al. 2001).

In the next section we discuss the origin of the He I emission in η Car and the implications of its absence prior to 1944.

6. The He I Emission Problem

According to the consensus view since 1998, η Car is probably a binary system with a highly eccentric 5.5-year orbit. In most discussions the hypothetical hot, massive companion

star, which has not been detected *per se*, serves three purposes: (1) Its wind collides with the primary wind in order to produce the observed X-rays, (2) it provides a basis for the 5.5-yr period, and (3) it supplies far-UV photons which indirectly cause the observed He I, [Ne III], and [Fe III] emission lines. However, *the absence of such features before 1944 is not easy to explain in models that invoke a hot secondary star*. This is particularly true for the broad He I lines. In the previous section we discussed the progressive changes in the wind of η Car. In this section we describe the special difficulties concerning the helium emission.

Since the present-day He I features have broad varying profiles and the locations of their strongest emission are spatially unresolved in Hubble Space Telescope (HST) data, they almost certainly originate less than 100 AU from the star. Being recombination lines, they are produced in zones of ionized He rather than neutral He. (Forbidden high-excitation lines such as [Ne III] and [Fe III] originate in lower-density ionized He zones farther out, see Davidson et al. (1995) and spectra in the HST archives.⁹) Figure 12 indicates the most relevant locations for ionized He if a hot, massive companion star is present. This refers to the “normal” situation, not near the time of a spectroscopic event. Objects A and B are the two stars, usually 15–30 AU apart; C (filling most of the figure) is the dense primary wind; region D is the faster, lower-density secondary wind; and E is the shocked region between the winds. Proposed ionized He zones include:

1. Region 1, the hot inner part of the primary wind. The observed He I brightness is difficult to explain in a spherical wind model (Hillier et al. 2001), but Smith et al. (2003b) found strong evidence that the wind is latitude-dependent, not spherical. The lower-density, hotter equatorial region may produce appreciable He I emission without the assistance of a companion star.
2. Region 2, a photoionized He zone in the dense primary wind, adjoining the shocked region. It has long been recognized that a hot secondary star would create such a zone (Davidson 2001a,b) and a qualitative scenario has recently been mentioned by Nielsen et al. (2007). This is probably the most popular choice at present.
3. If the secondary star is reasonably normal and less than 3 million years old (consistent with the massive primary), then its wind is not a promising source for η Car’s present-day He I lines. The winds of normal 30–60 M_{\odot} stars at moderate stages of evolution are not dense enough to convert more than small fractions of the far-UV radiation, and their high wind speeds cause very broad line profiles. Kashi & Soker (2007), however,

⁹ <http://etacar.umn.edu/> and <http://archive.stsci.edu/prepds/etacar/>.

have described a model wherein they *assumed* that He I emission arises in the small, dense acceleration zone of the secondary wind, location 3 in our sketch.

4. The shocked region between the winds generally contains He^{++} rather than He^+ and has high temperatures, unfavorable for recombination emission. If the cooling rate is sufficiently fast, though, some localized gas may cool below 10^5 K before moving far. The result would be a chaotic ensemble of photoionized cloudlets or filaments with ionized He at temperatures of the order of 15000 K, amid the uncooled shocked gas hotter than 10^6 K. Such condensations would be very small and dense due to approximate pressure balance within region E. This possibility is indicated by label 4 in Fig.12.
5. Smith et al. (2003b) speculated that ionizing photons might come from low latitudes in the primary wind’s pseudo-photosphere, instead of a hot companion star. If so, then such radiation may ionize the low-latitude wind out to large radii. This idea is not shown in Fig.12, because the geometry would be different.

Any successful model for the present-day He I features must account for their weakness or absence before 1944. Suppose that a hot secondary star ($T_{\text{eff}} > 32000$ K) supplies the helium-ionizing photons. Motivated by the nature of the observed spectroscopic cycle, most authors have favored a highly eccentric 5.5-year orbit wherein the apastron and periastron separations are, respectively, about 30 AU and less than 6 AU. As we noted in §5, obscuration by circumstellar dust plays almost no role in the following discussion, since the radiation density within 100 AU of η Car is too high for dust grains to exist there.

The spectroscopic events now observed at 5.5-year intervals involve, among other effects, a temporary fading of all emission lines that originate in the ionized He regions. Each spectroscopic event resembles what one would expect to see if the periastron approach of star B triggers a massive enhancement of the primary wind at low latitudes. Helium-ionizing radiation from B can temporarily disappear within the pseudo-photosphere because the entire configuration is then small and dense, only a few AU across. Similar suggestions have been expressed by Zanella et al. (1984), Davidson (1999), Smith et al. (2003b), and Martin et al. (2006a). Independent of whether this general idea is the right explanation for the observed events, it cannot account for a *long-term* weakness or absence of the He I lines, as we explain in the next paragraph.

The basic difficulty is that hypothetical star B spends most of its time farther than 15 AU from the primary, at radii where no credible wind can obscure the ionized He zones. The primary wind may have been denser before 1944 than it is today, particularly at low latitudes as emphasized by (Smith et al. 2003b). High densities would not have prevented

star B from ionizing helium in region 2 of Fig. 12, and the standard efficiency for converting far-UV photons to helium recombination emission depends only weakly on density (Osterbrock & Ferland 2006). Suppose, therefore, that we try to hide the He I recombination lines by continuum absorption and scattering in the dense wind. Region 2 in Fig. 12 is usually at distances of 15 to 35 AU from the primary. In order to produce a Thomson-scattering optical depth of unity outside $r \sim 25$ AU, a spherical model with a wind speed of 500 km s^{-1} would need a mass-loss rate of about $0.01 M_{\odot} \text{ yr}^{-1}$, ten times the present-day value. But this amount of scattering would merely distort the emission line profiles. In order to suppress or conceal them, either the optical depth for scattering must be very large, or, more likely, absorption must be strong enough that the “thermalization optical depth” is substantial, $\sqrt{3\tau_{\text{abs}}\tau_{\text{tot}}} \gtrsim 1$, around the ionized He region. This would automatically create a pseudo-photospheric radius of the order of 25 AU, implying an effective temperature less than 4500 K for the entire configuration. Such a model is unlikely for several reasons:

- It would be even larger and cooler than the state seen in the second eruption, e.g. around 1893. In that case one does not expect to see the emission-line spectrum that was observed in 1900–1941, described elsewhere in this paper and qualitatively resembling the present-day forest of Fe II, [Fe II], and Ni II emission lines.
- Relevant opacities decline rapidly at temperatures below 7000 K; this is why supernova explosions and major LBV eruptions have pseudo-photospheres around 7000 K (Davidson 1987). Therefore, if the hypothetical opaque gas was cooler than 5000 K as one would expect from the size scale and η Car’s luminosity, then it must have been several orders of magnitude denser than present-day conditions, in order to have sufficient optical depth. This would imply a tremendous 1900–1940 mass-loss rate whose ejecta should have been obvious today.¹⁰ Larger opacities would have required higher temperatures, 6000–10000 K at locations $r > 15$ AU. Opaque gas with $T > 6000$ K obviously did not surround the star at $r > 15$ AU, because the emergent luminosity would have exceeded $10^7 L_{\odot}$, more than twice the present-day total for η Car. Thus we must imagine a localized absorbing region, but its characteristic diameter had to be at least 10 AU in order to hide zone 2 in Fig. 12. It would have radiated more than $10^6 L_{\odot}$, while covering only a small fraction of the solid angle around η Car – in other words, one must explain how enough energy was channeled through such a region to heat it.

¹⁰ A detailed quantitative discussion of this point would be beyond the scope of this paper because the theoretical situation is complex. However, our comments are illustrated by giant LBV eruptions, see Humphreys & Davidson (1994). The “Weigelt blobs” located several hundred AU from η Car are not massive enough to be the 1900–1940 ejecta in this type of model, see Davidson et al. (1995).

- With temperatures of 4000–10000 K as mentioned above, the hypothetical opaque gas would have radiated mainly at blue-to-red wavelengths, not in the UV as η Car does today. Since it would have been intrinsically very bright at photographic and visual wavelengths, at least 5 magnitudes of circumstellar and interstellar extinction would have been required in order to explain the 8th-magnitude appearance seen before 1940. A strongly obscured, relatively cool radiator would have appeared very red, $B - V > 2$, contrary to the observations (including the objective prism spectra).

The same considerations apply to region 4 in Fig. 12. A resourceful theorist might overcome these difficulties by carefully adjusting the geometry and other parameters, but *no quantitative model of this type has yet been proposed*.

As we remarked earlier, the fast secondary wind is an unlikely source for the observed He I emission. Normal O-type stars do not produce He I lines with strengths and profiles comparable to those now seen in η Car. Kashi and Soker (2007) nevertheless propose that the region of interest is in the acceleration zone of the secondary wind, a locale with radius less than 0.2 AU. Maybe the primary star and its wind somehow alter the physical conditions there. If so, then those conditions may have been different before 1940; the arguments listed above do not apply to a source region smaller than several AU. One obvious objection to this scenario, however, is that the *inner* wind of a massive O-type star should be physically robust in this context. The acceleration zone’s ram pressure, gas density, radiation density, and ambient temperature considerably exceed the values found in nearby regions of the primary wind at most phases of the orbital cycle. (If they do not, then a colliding-wind model has difficulty explaining the X-rays, see Pittard & Corcoran 2002.) A substantial perturbation of the inner secondary wind, needed in order to produce strong He I emission there, would evidently require some special, rather surprising effect. Moreover, if the secondary wind accounts for the present-day He I lines, then one must explain why zones 2 and 4 in Fig. 12 – the large “obvious” regions for He I emission – are ineffective.

Alternatively one might invoke some unusual type of secondary star or secondary wind; but such models are unappealing because they require two peculiar objects together.

In summary, one cannot explain the pre-1944 absence of He I lines merely by supposing that “the ionized He region was obscured” or “outflowing material engulfed the companion star.” *If a hot secondary star provides most of the helium-ionizing photons, then some additional effect is required in order to explain the pre-1944 weakness of the helium features.*

One aspect of helium recombination may help. In the following account, we employ atomic parameters quoted by Osterbrock & Ferland (2006) and parameters for η Car consistent with various observations (Davidson & Humphreys 1997). This is an order-of-

magnitude outline in order to put the problem in context; we plan a future, more detailed discussion of the present-day He I intensities and velocity profiles. The threshold for photoionization of helium in its ground level $1s^2\ ^1S$ is $\epsilon \approx 24.6$ eV or $\lambda \approx 504$ Å. Most helium recombination events create atoms in excited triplet states, which then decay in one or more steps to the metastable $1s2s\ ^3S$ level about 19.8 eV above the ground state. For densities of interest here, subsequent decay to the singlet ground level is enabled mainly by collisional transitions from $1s2s\ ^3S$ to the $1s2s$ and $1s2p$ singlet states. If this were the whole story, then the average lifetime of the $\text{He}^0\ 1s2s\ ^3S$ level would be of the order of 0.1 s at radius $r \sim 25$ AU in η Car’s present-day wind.

However, that level can be ionized by near-UV photons having $\epsilon > 4.8$ eV and $\lambda < 2600$ Å. Given the present-day spectrum of η Car, this should usually occur in a time less than 0.001 s at the location mentioned above – much faster than transitions to singlet states. In an ionized zone near η Car, therefore, most triplet recombination events do not create ground-level helium atoms. If we count only singlet recombination events, the effective recombination coefficient for $\text{He}^+ \rightarrow \text{ground-level He}^0$ is thereby reduced by a factor of roughly 4 compared to standard nebular conditions. The volume extent of an ionized He zone is consequently larger than one would estimate from a Zanstra calculation based on photons above 24.6 eV and total recombination coefficients. Meanwhile the triplet recombination events *do* lead to decays which produce emission lines, including $\lambda 4471.5$. Result: *For a given amount of radiation above 24.6 eV, η Car’s present-day wind produces far more helium recombination emission than one would naively expect.*

Conceivably we can explain the pre-1944 He I emission-line deficit by supposing that the standard textbook recombination coefficient was valid at that time, thereby reducing the extent of the ionized He zones. In other words, maybe the $1s2s\ ^3S$ re-ionization effect described above occurs today but was ineffective before the 1940’s. Here are two possible reasons:

- If η Car’s mass-loss rate was quite high at that time, then the pseudo-photospheric surface in the opaque primary wind would have been larger and cooler than it is today. Maybe it produced very little radiation capable of ionizing $\text{He}^0\ 1s2s\ ^3S$ ($\epsilon > 4.8$ eV, $\lambda < 2600$ Å).
- Higher densities in the ionized region would have increased the rate for collisional transitions from $1s2s\ ^3S$ to singlet states. This would be especially true if the present-day ionized He zone is region 2 of Fig. 12, but before 1944 it was in region 4 because cooling was faster then. As noted above, small condensations of cooled material can have very high densities within the shocked region.

These suggestions do not solve the problem, though, since at least three objections must be overcome:

- Independent of the primary star, the hypothetical companion star can also ionize He^0 $1s2s\ ^3\text{S}$. For every type of proposed object, photons above 4.8 eV far outnumber those above 24.6 eV.
- The estimated ratio of rates for depopulating the $1s2s\ ^3\text{S}$ level,

$$r(\text{photoionization})/r(\text{collisional}),$$

must be decreased by a large factor, on the order of 300, in order to make triplet recombination events effective in populating the ground level.

- The effect that we have described can change the amount of ionized He by a factor of about 4 but not much more. As discussed in §4 above, the He I $\lambda 4471$ line may be present in the 1938 spectrum with at most one-fourth its strength in 1944-51 (relative to other emission lines), but the data actually support a lower value.

Now suppose we consider a different possibility, that η Car’s present-day He I lines are excited by the primary star and have nothing to do with a companion – i.e., cases 1 and 5 in our list of He^+ locations. Then the pre-1944 spectra present no serious difficulty concerning helium; a modest increase in the wind density, or a change in latitude structure as suggested by Smith et al (2003b) and Davidson (2005), would suppress helium-ionizing photons and emergent He I emission lines (see §5.4). Since this would occur in the inner wind, $r < 6$ AU, the difficulties noted above would not apply. In a model of this type the high excitation lines in general, e.g. [Ne III] and [Fe III], may be unrelated to any hypothetical secondary star.

In summary: Given that He I emission lines have been quite obvious in η Car since the mid-1940’s, *their weakness or absence before that time is difficult to explain in models that employ a companion star to supply the far-UV photons*. We do not claim that this argument disproves the concept of a hot secondary star, but it does imply that the popular binary scenario requires additional justification which no one has yet offered. So far, many qualitative ideas have been proposed for η Car’s spectroscopic behavior but there are no realistic, quantitative *models*.

7. Conclusions

Our measurement and analysis of the Harvard objective prism spectra of η Car from 1902 to 1941, has shown that He I 4471\AA emission may be marginally present, but no

stronger than about one-fourth of its relative intensity as estimated by Gaviola in spectra from 1944-51. Our results are equally consistent with no contribution from the He I $\lambda 4471$ line. The [Fe III] high excitation lines are either absent or very weak in these spectra. The star was thus always in the “low excitation” state and there were no apparent spectroscopic events from the time of the second eruption in the 1890’s to 1944.

Obscuration of the proposed companion star by either dust or an optically thick wind cannot explain the lack of He I emission prior to 1944. We discussed the possible sources of He I emission in the η Car system and demonstrated that it is very difficult to explain its absence if the UV flux comes from the proposed hot secondary star. Alternatively, we suggest that the equatorial wind of the primary may be the source of the UV flux due to η Car’s post-eruption rotational spin-up and the onset of its present bipolar wind, coincident with its brightening between 1940 and 1952 (Smith et al. 2003b).

This work has also demonstrated that with careful processing and calibration these historical spectra are quite useful especially for objects of astrophysical interest.

RMH is especially grateful to Alison Doane, Tracy McGinnis and Martha Hazen at CfA for their assistance with the plate collection and for digitizing several of the plates. We also thank John Hillier for sharing his 1986 spectrum of η Car with us, and Nolan Walborn for comments on his identifications in Le Sueur’s 1870 spectrum.

A. The Harvard Objective Prism Plates of Eta Car

For future reference, we provide a chronological list of all the Harvard objective prism plates with spectra of η Car in Table A1 that we examined including comments on the spectra, the image quality, and in some cases whether the plate was missing or broken.

REFERENCES

- Aller, L. H. & Dunham, T., Jr. 1966, ApJ, 146, 126
- Bidelman, W. P., Galen, T. A. & Wallerstein, G. 1993, PASP, 105, 785
- Bok, B. J. 1930, Pop. Astr., 38, 399
- Cannon, A. J. 1901, Harvard Ann., 28, 175
- Damineli, A. 1996, ApJ, 460, L49

- Damineli, A., Kaufer, A., Wolf, B., Stahl, O., Lopes, D. F. & Araujo, F. 2000, ApJ, 528, L101
- Davidson, K. & Ruiz, M. T. 1975, ApJ, 202, 421
- Davidson, K. & Humphreys, R. M. 1986. A&A, 164, L7
- Davidson, K. 1987, ApJ, 317, 760
- Davidson, K., Ebbets, D., Wiegelt, G., Humphreys, R.M., Hajian, A.R., Walborn, N.R., & Rosa, M. 1995, AJ, 109, 1784
- Davidson, K., & Humphreys, R.M. 1997, ARA&A, 35, 1
- Davidson, K. 1999, in ASP Conf. Ser. 179, “Eta Carinae at the Millennium”, ed. J.A. Morse, R.M. Humphreys, & A. Damineli, (San Francisco, ASP), p. 304
- Davidson, K. et al. 1999, AJ, 118, 1777
- Davidson, K., Ishibashi, K., Gull, T. R., Humphreys, R. M., & Smith, N. 2000, ApJ, 530,
- Davidson, K. 2001a, in ASP Conf. Ser. 233, “P Cygni 2000”, ed. M. de Groot & C. Sterken, (San Francisco, ASP), p. 173
- Davidson, K., 2001b, in ASP Conf. Ser. 242, “Eta Carinae and Other Mysterious Stars: The Hidden Opportunities of Emission Line Spectroscopy”, ed. T. R. Gull, S. Johansson, & K. Davidson (San Francisco, ASP), p. 3
- Davidson, K., Smith, N., Gull, T. R., Ishibashi, K., & Hillier, D. J 2001, AJ, 121, 1569
- Davidson, K. 2005, in ASP Conf.Ser. 332, “The Fate of the Most Massive Stars”, ed. R. Humphreys & K. Stanek (San Francisco, ASP), p. 101
- Davidson, K. et al, 2005, AJ, 129, 900
- de Vaucouleurs, G. & Eggen, O. C. 1952, PASP, 64, 185
- Feast, M. W., Whitelock, P. A., & Marang, F. 2001, MNRAS, 322, 741
- Gaviola, E. 1953, ApJ, 118, 234
- Gill, D 1901, MNRAS, 61, 66
- Glatzel, W. 2005, in ASP Conf.Ser. 332, “The Fate of the Most Massive Stars”, ed. R. Humphreys & K. Stanek (San Francisco, ASP), p. 22

- Hillier, D. J. & Allen, D. 1992, *A&A*, 262, 153
- Hillier, D. J., Davidson, K., Ishibashi, K. & Gull, T. 2001, *ApJ*, 553, 837
- Hillier, D. J., et al. 2006, *ApJ*, 642, 1098
- Hoffleit, D. 1933, *Harvard Bull.*, No. 893, 11
- Humphreys, R. M. 1999, in *ASP Conf.Ser* 179, “Eta Carinae at the Millenium”, ed. J. Morse, R. Humphreys & A. Damineli (San Francisco, ASP), p. 280
- Humphreys, R. M. & Davidson, K. 1994, *PASP*, 106, 1025
- Humphreys, R. M., Davidson, K. & Smith, N. 1999, *PASP*, 111, 1124.
- Humphreys, R. M. & Koppelman, M. 2005, in *ASP Conf.Ser.* 332, “The Fate of the Most Massive Stars”, ed. R. Humphreys & K. Stanek (San Francisco, ASP), p. 159
- Iping, R. C., Sonneborn, G., Gull, T. R., Massa, D. L., & Hillier, D. J. 2005, *ApJ*, 633, 371
- Ishibashi, K. 2001, in *ASP Conf. Ser.* 242, “Eta Carinae and Other Mysterious Stars: The Hidden Opportunities of Emission Line Spectroscopy”, ed. T. R. Gull, S. Johansson, & K. Davidson (San Francisco, ASP), p. 53
- Ishibashi, K. et al. 2003, *AJ*, 125, 3222
- Kashi, A., & Soker, N. 2007, *New Astronomy*, 12, 590
- Le Sueur, A. 1870, *Proc. Roy. Soc.*, 18, 245
- Lunt, J. 1919, *MNRAS*, 79, 621
- Martin, J. C. & Koppelman, M. 2004, *AJ*, 127, 2352
- Martin, J. C., Davidson, K., Humphreys, R. M., Hillier, D. J., & Ishibashi, K. 2006a, *ApJ*, 640, 474
- Martin, J. C., Davidson, K. & Koppelman, M. 2006b, *AJ*, 132, 271
- Moore, J. H. & Sanford, R. F. 1913, *Lick Obs. Bull.*, 8, 55
- Moore, J. H. & Sanford, R. F. 1916, *Lick Obs. Bull.*, 8, 134
- Morris, P. W., et al. 1999, *Nature*, 402, 502

- Nielsen, K.E., Corcoran, M.F., Gull, T.R., Hillier, D.J., Hamaguchi, K., Ivarsson, S., & Lindler, D.J. 2007, *ApJ*, 660, 669
- O’Connell, D. J. K., S.J. 1956, *Vistas in Astronomy*, 2, 1165
- Osterbrock, D.E., & Ferland, G.J. 2006, *Astrophysics of Gaseous Nebulae and Active Galactic Nuclei* (University Science Books, Sausalito)
- Owocki, S. 2005, in *ASP Conf.Ser. 332*, “The Fate of the Most Massive Stars”, ed. R. Humphreys & K. Stanek (San Francisco, ASP), p. 169
- Pittard, J. M. & Corcoran, M. F. 2002, *A&A*, 383, 636
- Rodgers, A. W. & Searle, L. 1967, *MNRAS*, 135, 99
- Schuster, A. 1872, *Proceedings of the Royal Society of London*, Vol. 20, 484
- Shaviv, N. 2005, in *ASP Conf.Ser. 332*, “The Fate of the Most Massive Stars”, ed. R. Humphreys & K. Stanek (San Francisco, ASP), p. 180
- Smith, N. & Gehrz, R. D. 1998, *AJ*, 116, 823
- Smith, N., et al. 2003a, *AJ*, 125, 1458
- Smith, N., Davidson, K., Gull, T. R., Ishibashi, K. & Hillier, D. J. 2003b, *ApJ*, 586, 432
- Smith, N. 2005, *MNRAS*, 357, 1330
- Stahl, O., Weis, K., Bomans, D. J., Davidson, K., Gull, T. R., & Humphreys, R. M. 2005, *A&A*, 435, 303
- Thackeray, A. D. 1953, *MNRAS*, 113, 211
- Thackeray, A. D. 1967, *MNRAS*, 135, 51
- van Boekel, R. et al. 2003, *A&A*, 410, L37
- Viotti, R. 1968, *Mem. Soc. Ast. It.*, 39, 105
- Walborn, N. R. & Liller, M. *ApJ*, 211, 181
- Whitelock, P. A., Feast, M. W., Carter, B. S., Roberts, G. & Glass, I. S. 1983, *MNRAS*, 203, 385
- Whitelock, P. A., Feast, M. W., Koen, C., Roberts, G., & Carter, B. S. 1994, *MNRAS*, 270, 354

Whitney, C A. 1952, Harvard Bull., No. 921, p.8

Zanella, R., Wolf, B., & Stahl, O. 1984, A&A, 137, 79

Zethson, T. 2001, Ph.D Thesis, Lund Universitet, Sweden

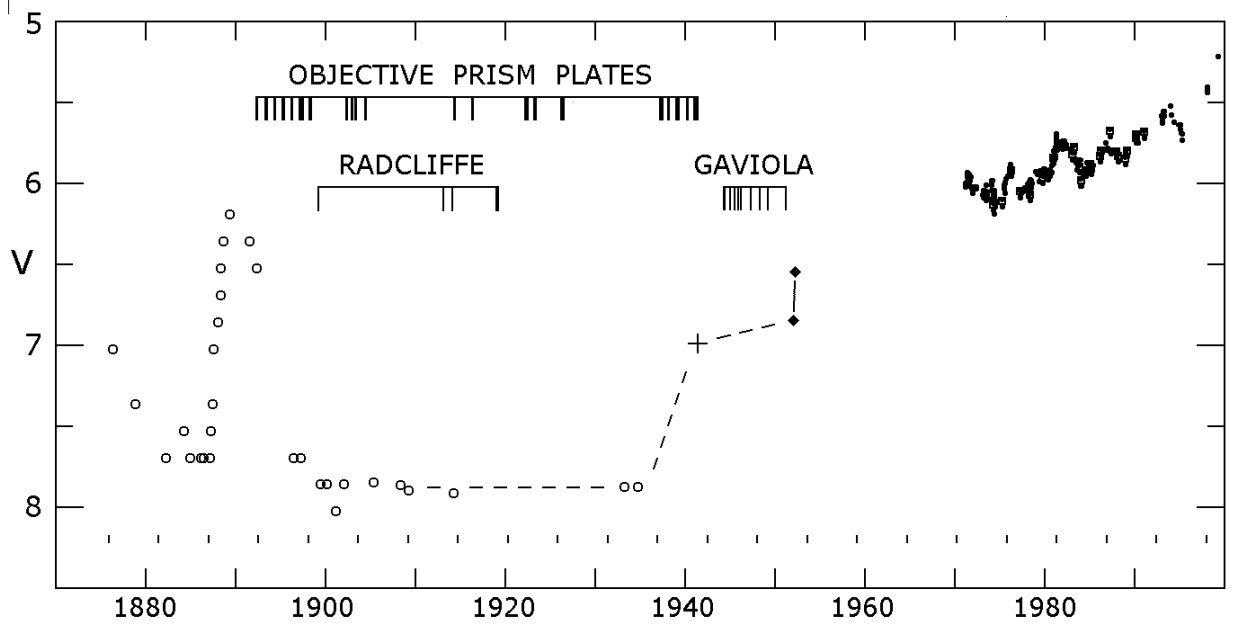


Fig. 1.— The light curve of η Car from 1870 to the present showing the times of the early spectra. The small tick marks near the bottom indicate the times of spectroscopic events ($t = 2003.5 - 5.54N$). Events before 1948 were not observed and the period is not guaranteed to be constant.

Table 1. Harvard Objective Prism Plates

Series	Telescope	Plate Scale	Dates	Location
A Series	24-inch Bruce Doublet	$60'' \text{ mm}^{-1}$	1896 – 1926	Arequipa, Peru
...	1929 – 1950	Bloemfontein, South Africa
B Series	8-inch Bache Doublet	$179'' \text{ mm}^{-1}$	1891 – 1923	Arequipa, Peru
...	1930 – 1954	Bloemfontein, South Africa
X Series	13-inch Boyden Refractor	$42.4'' \text{ mm}^{-1}$	1891 – 1926	Arequipa, Peru
...	1930 – 1951	Bloemfontein, South Africa

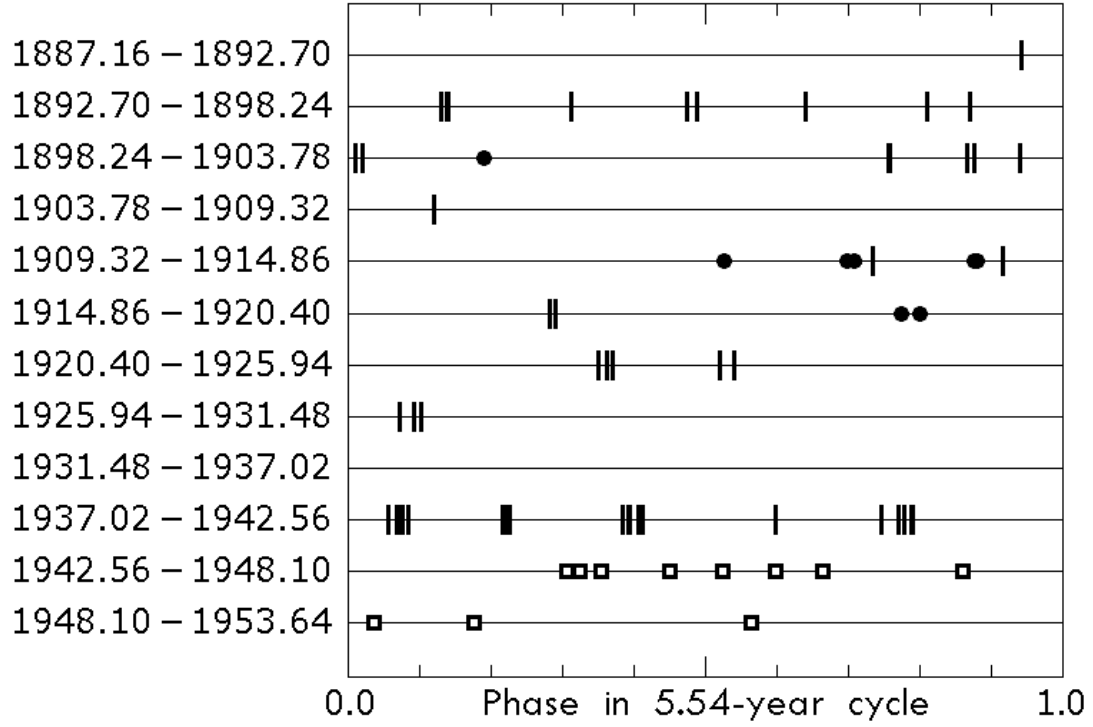


Fig. 2.— The phase of the early spectra in the 5.5 yr. cycle. The vertical marks are the Harvard objective prism spectra, the dots are Radcliffe spectra (Feast et al 2001), and the boxes are Gaviola's (1953) spectra.

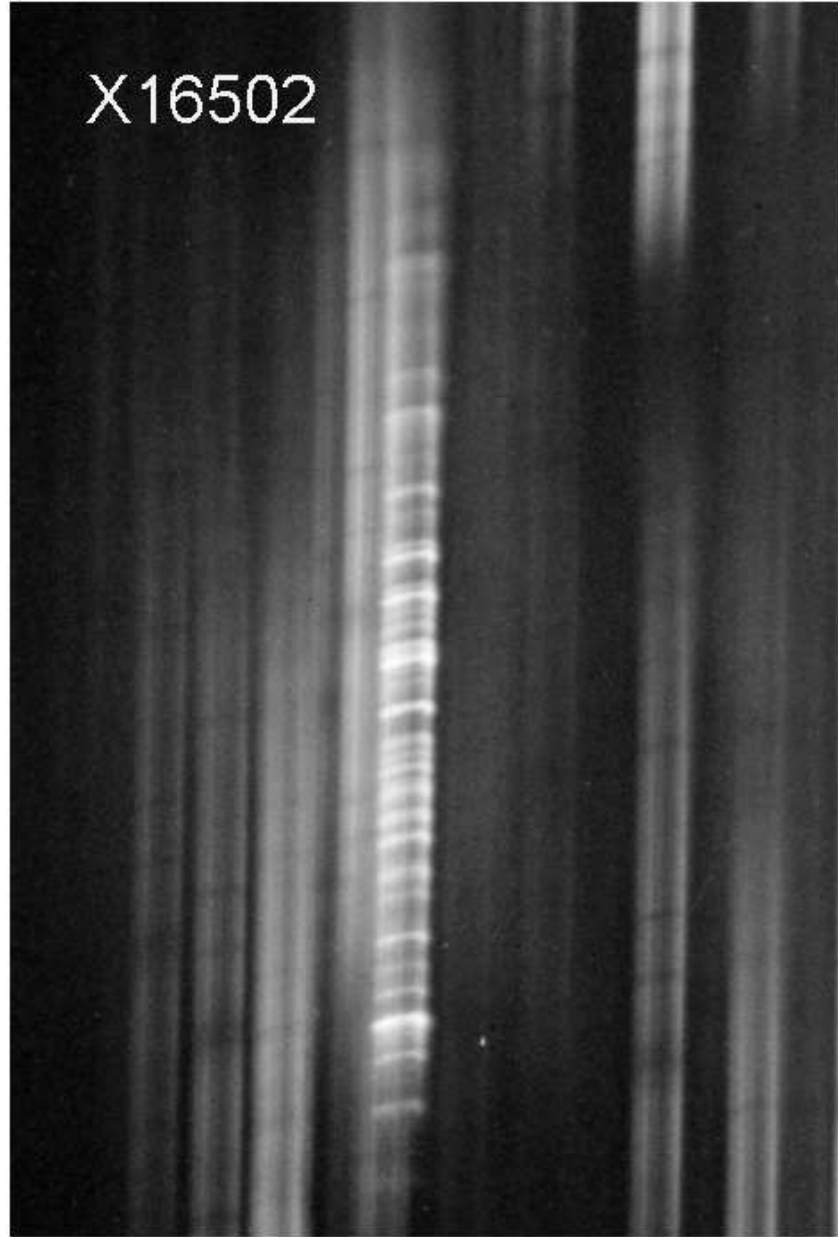


Fig. 3.— The digitized section of objective prism plate X16502; only a small fraction of the plate was digitized. Since this is a long exposure, the spectra of other nearby stars are conspicuous. The breadth of the spectrum perpendicular to the dispersion, caused by drifting the telescope, was slightly less than $1'$ in this example. Note that the dispersion direction is not exactly vertical in the digitized file.

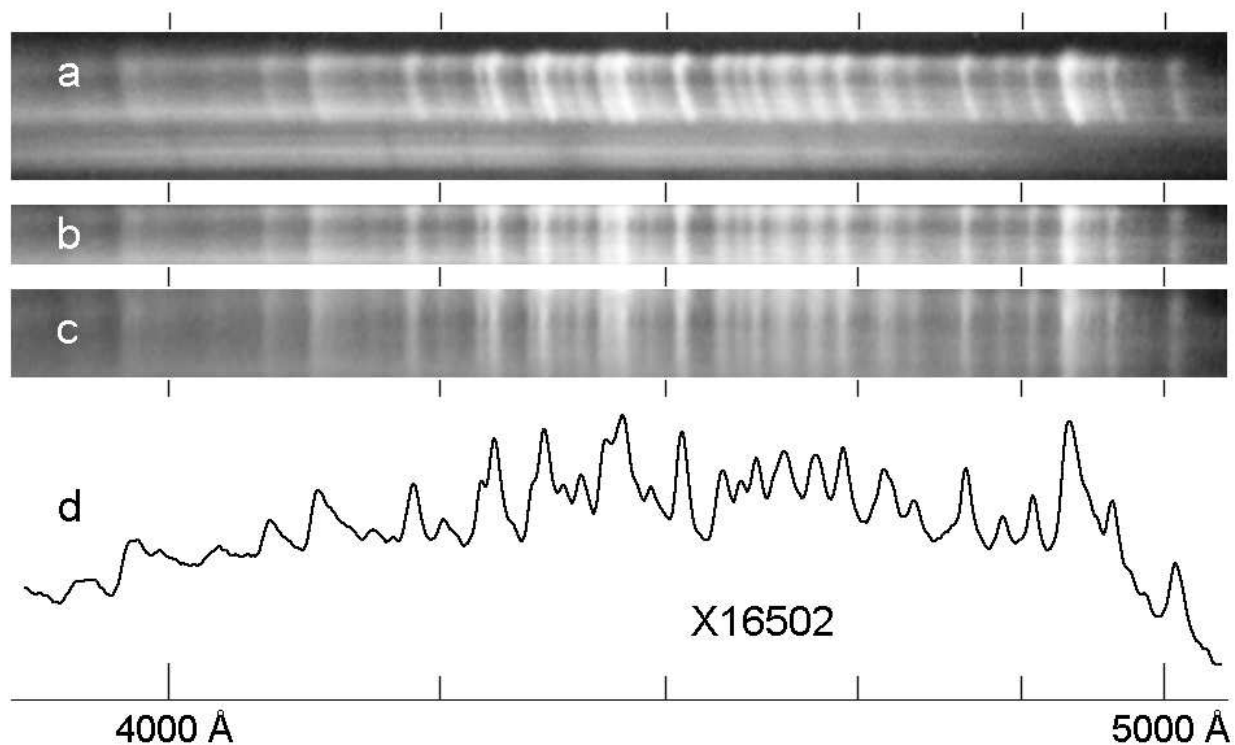


Fig. 4.— X16502. (a) The original digitized scan, like Fig. 3 but rotated so the dispersion direction runs exactly along rows of pixels. (b) Corrected for the curvature and other guiding problems as explained in the text. (c) Broadened perpendicular to the dispersion, and renormalized so that every row has the same average level. (d) The tracing of the spectrum, extracted by a procedure described in the text. Since the data are photographic with largely unknown parameters, the vertical scale is not linear. The tick marks in (a), (b), and (c) correspond to the same wavelength scale as (d). Plate X16502 was an unusually long exposure whose spectrum of η Car is of lower quality than most of the spectra used in our analysis. It was chosen here because it provides a clear example of our processing steps.

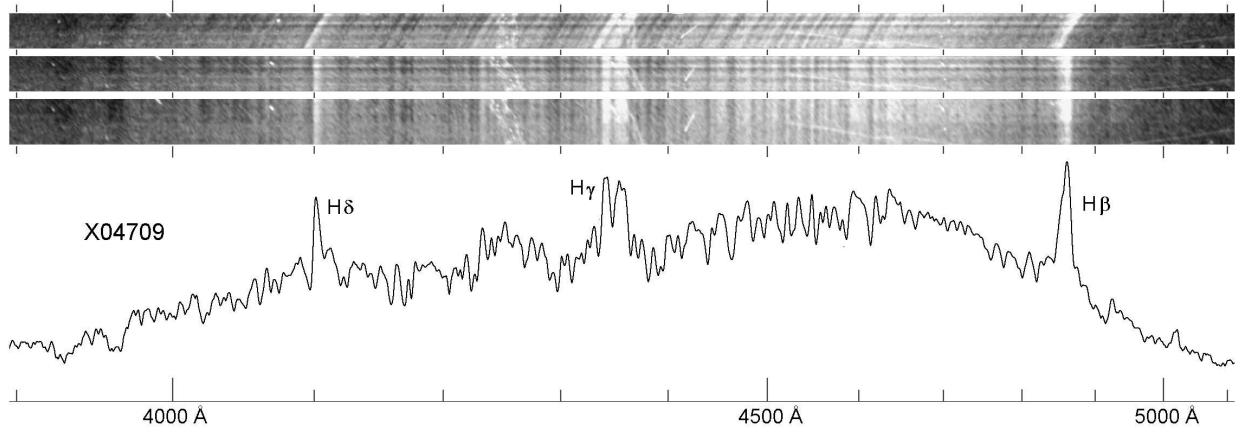


Fig. 5.— X04709, the famous spectrum from 1893 during η Car’s second eruption. The format is the same as figure 4. The upper spectrum indicates that the guiding was unusually steady for this plate. Most of the irregularities in the tracing are real spectral features, not noise. The plate has serious scratches in the emulsion near 4250 and 4360Å, but our processing techniques reduced their effects in the tracing.

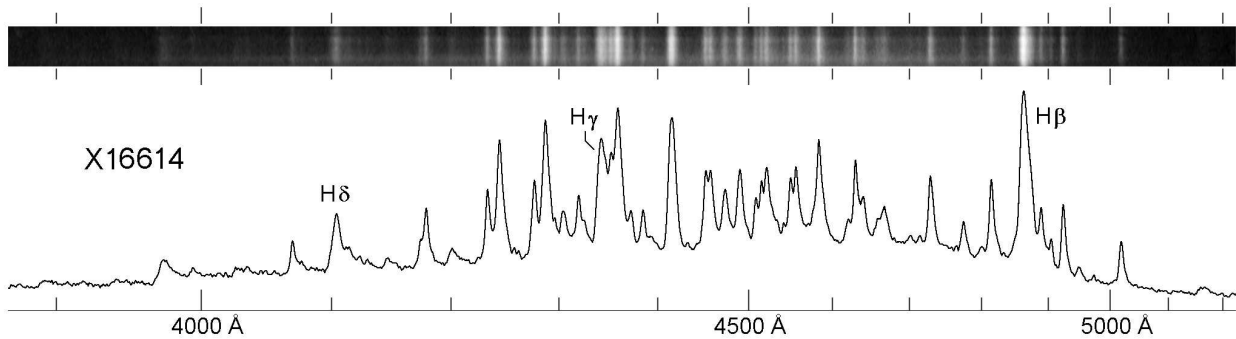


Fig. 6.— X16614(1938) is one of the best spectra in the objective prism series. The top spectrum shows the digitized scan rectified by our technique and the extracted tracing is shown below it.

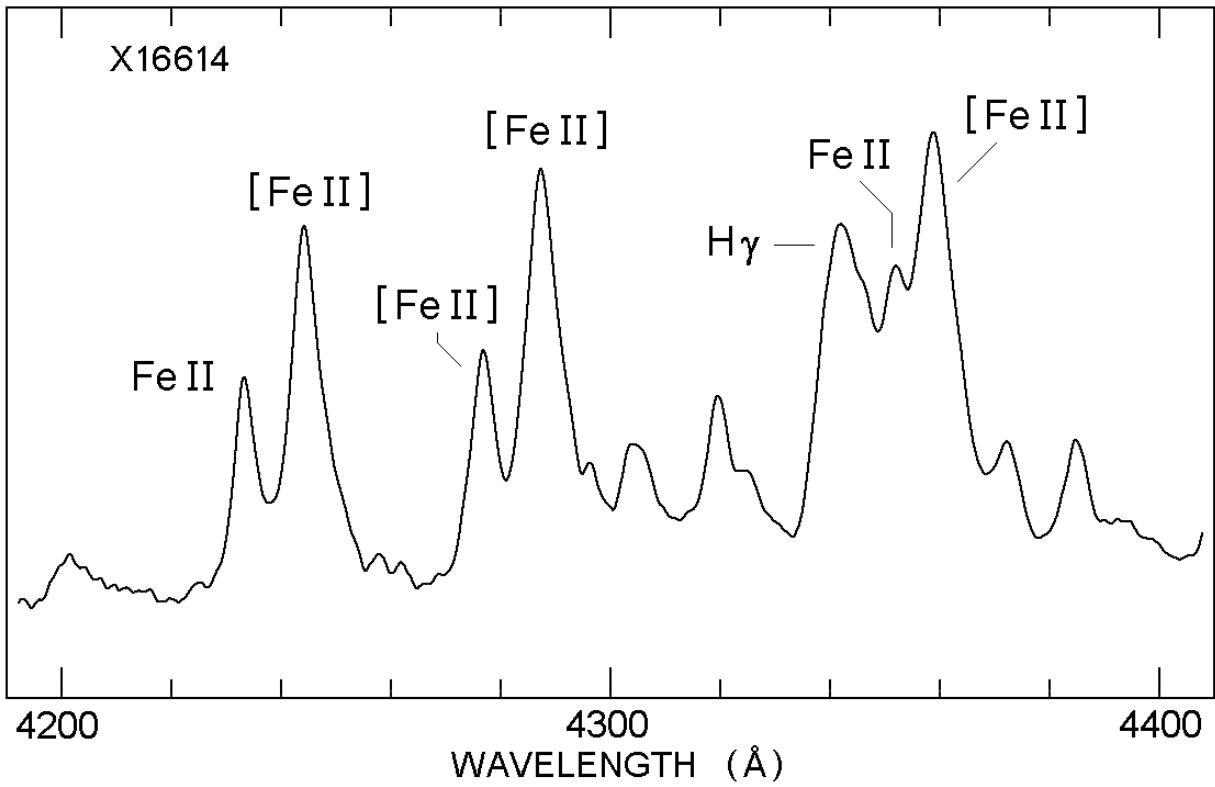


Fig. 7.— The spectral region around $H\gamma$ in X16614. Caveat: The vertical scale is non-linear because it represents photographic densities.

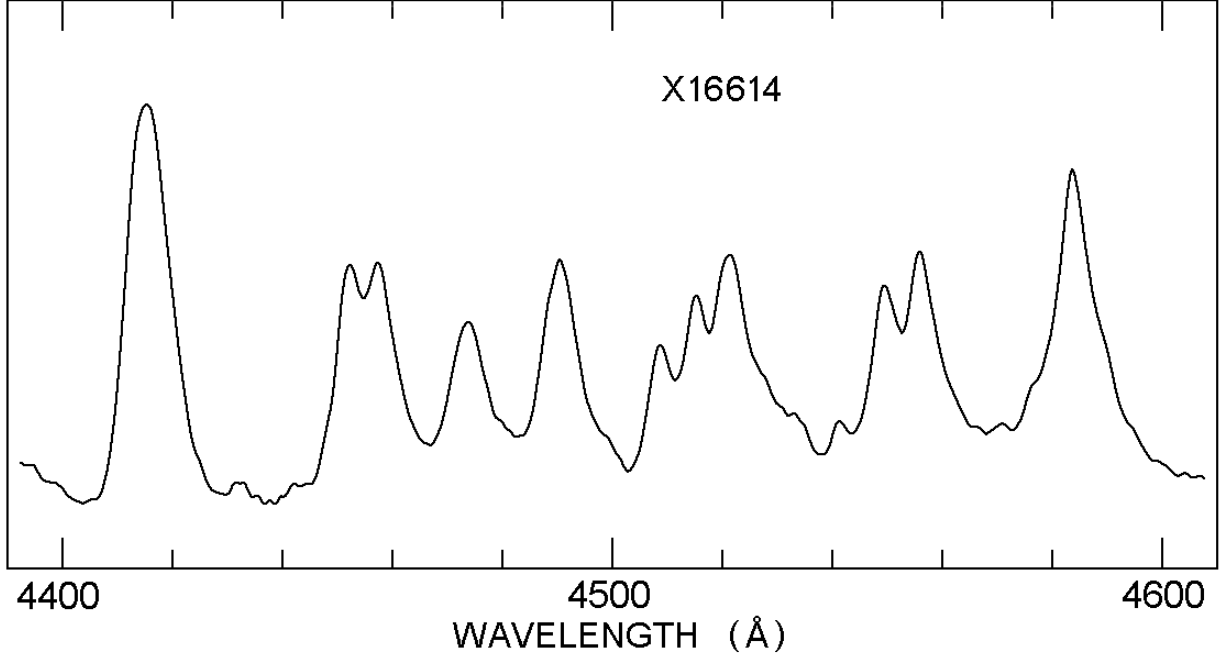


Fig. 8.— The main features shown here are all lines or blends of [Fe II] and Fe II. The region near 4470Å, where He I emission might appear, is shown in more detail in Fig. 9

Table 2. High Excitation Relative Line Strengths

Source	Date ^a	Phase	He I 4471.5/[Fe II] 4474.9	[Fe III] 4658/[Fe II] 4639.7
Gaviola (1953)	1944 - 1951	—	1	0.8
Thackeray(1953)	1951	.58	1.2	0.7
Aller & Dunham(1966)	1961	.39	1.2	1.0
Hillier & Allen ^b	1986	.88	1.1	1.2
Zethson (2001)	1999	.21	1.2	1.4
Gemini ^c	2007	.71	1.2	1.4

^aThe date of the observation(s)

^bSpectrum courtesy of John Hillier

^cFrom a spectrum obtained with GMOS on Gemini-S, June 2007

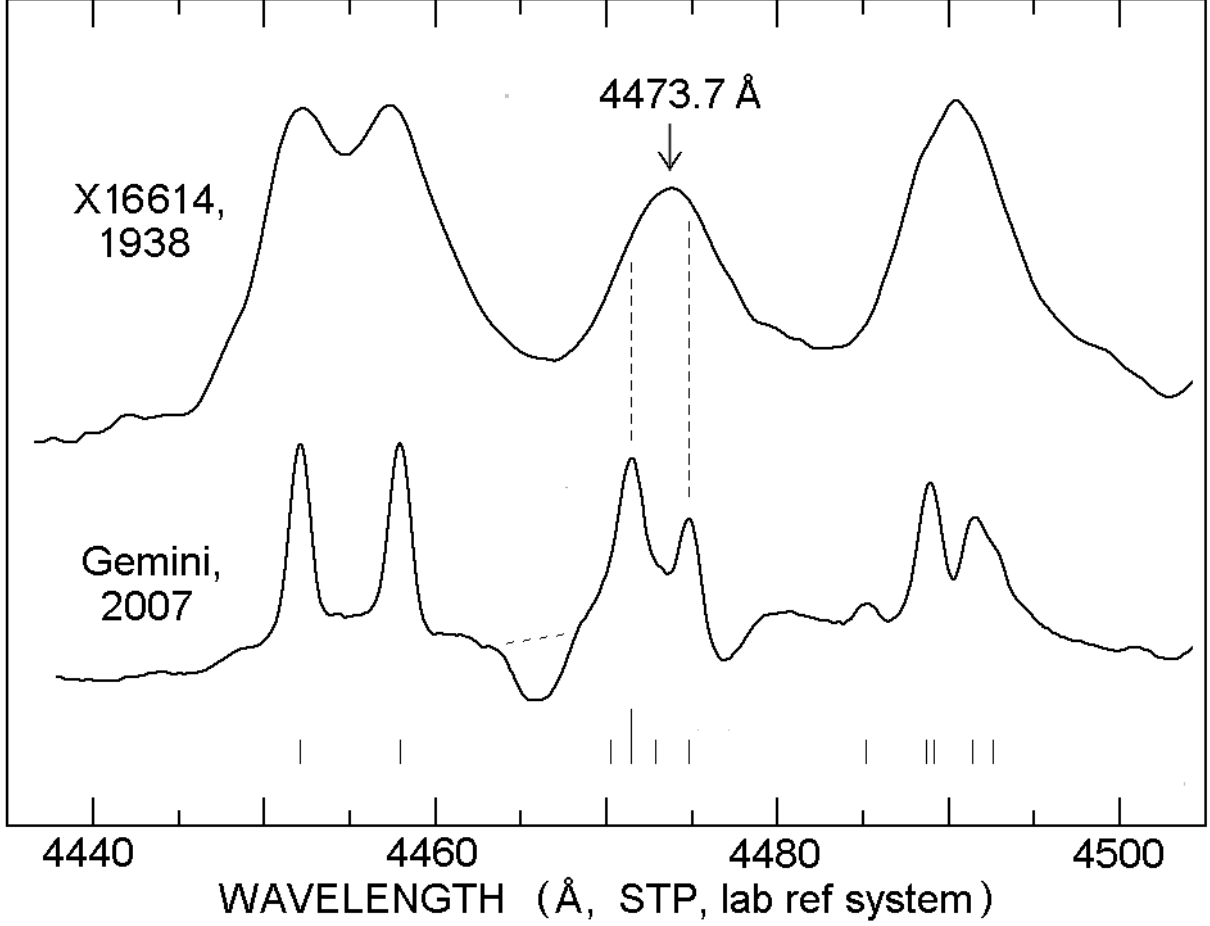


Fig. 9.— The upper spectrum shows the expanded spectrum of X16614 in the wavelength region of He I $\lambda 4471.5$. The vertical dashed lines mark the expected positions of He I $\lambda 4471.5$ and the [Fe II] line at 4474.9Å. The spectrum below it is the Gemini-S spectrum from June 2007. The narrow vertical lines mark the laboratory wavelengths of identified Fe II and [Fe II] lines in Aller & Dunham’s Coudé spectra. The dashed horizontal line in the Gemini spectrum marks the dip due to He I P Cygni absorption.

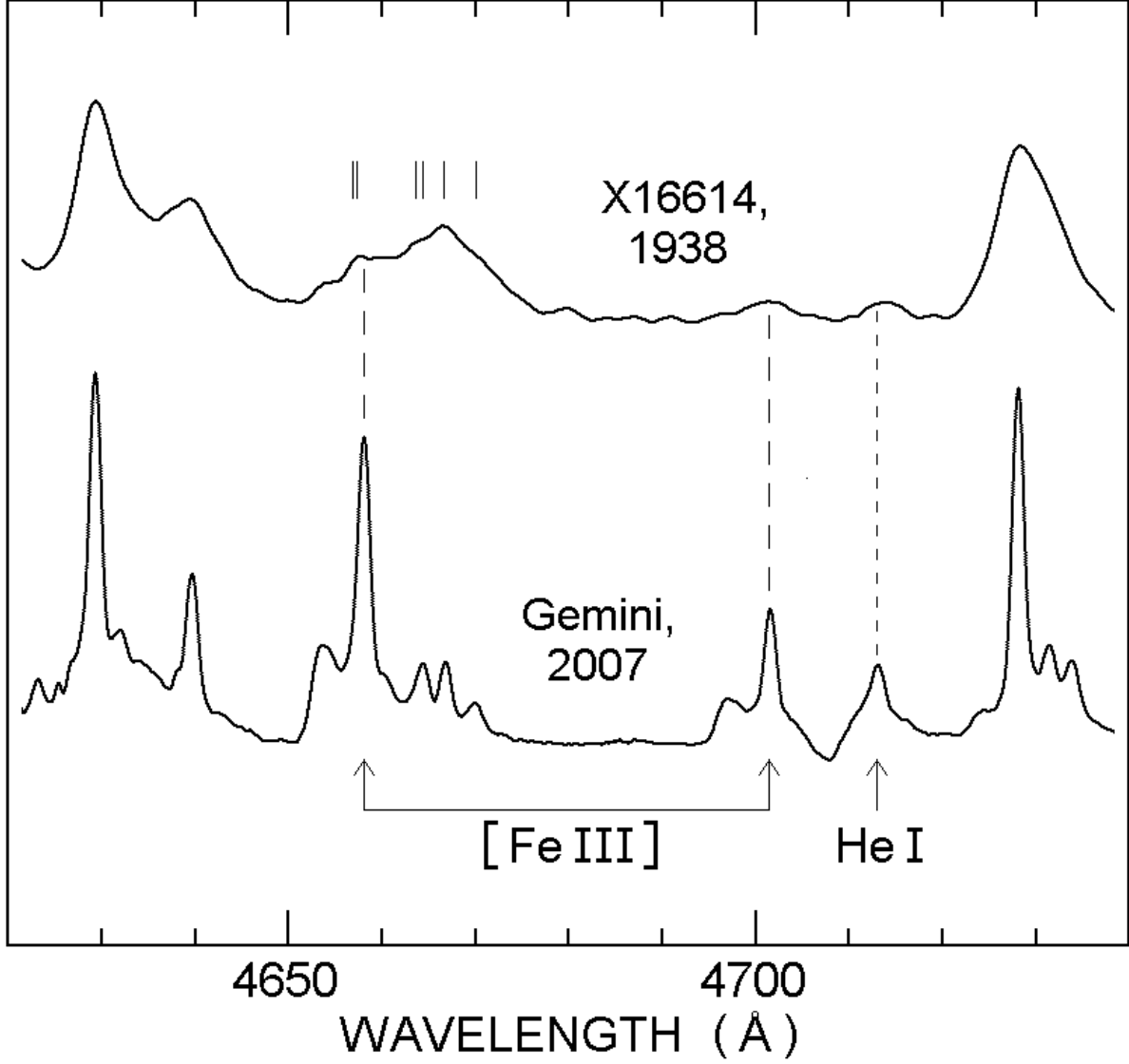


Fig. 10.— The expanded spectrum of X16614 in the region of the $[\text{Fe III}] \lambda 4658.1$ emission line. The tick marks at the top represent the low-excitation lines mentioned in the text, and several weak lines of Fe II and Cr II may also be contributing to the profile. The small bump in the X16614 spectrum at $\lambda 4701$ may be due to $[\text{Fe III}]$, but the other weak feature to its red does not match the He I line in wavelength.

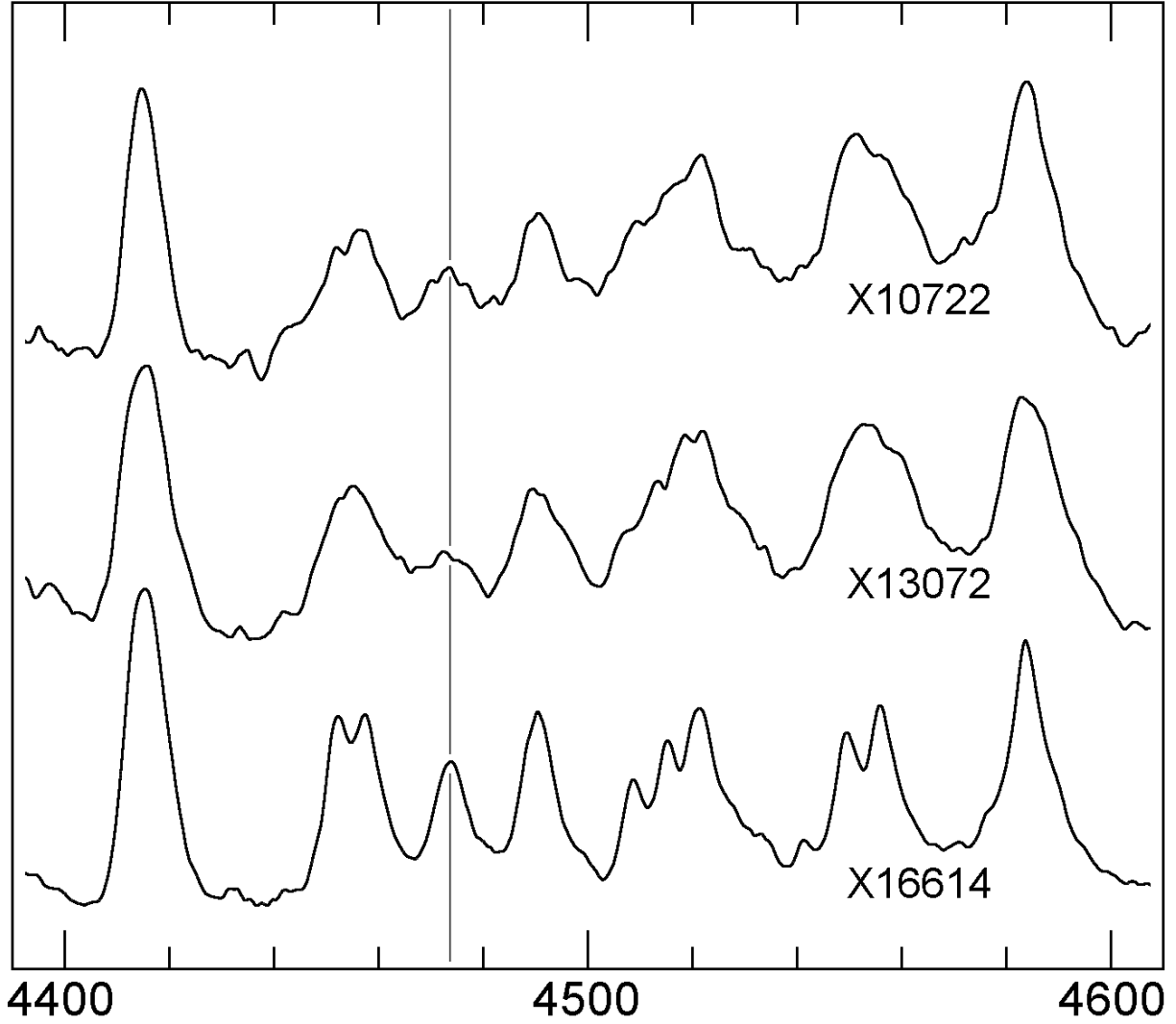


Fig. 11.— Two early spectra, X10722 (1903) and X13072 (1916) together with X16614 in the region of the $\lambda 4473$ emission feature. The vertical line marks the wavelength 4473.7 Å.

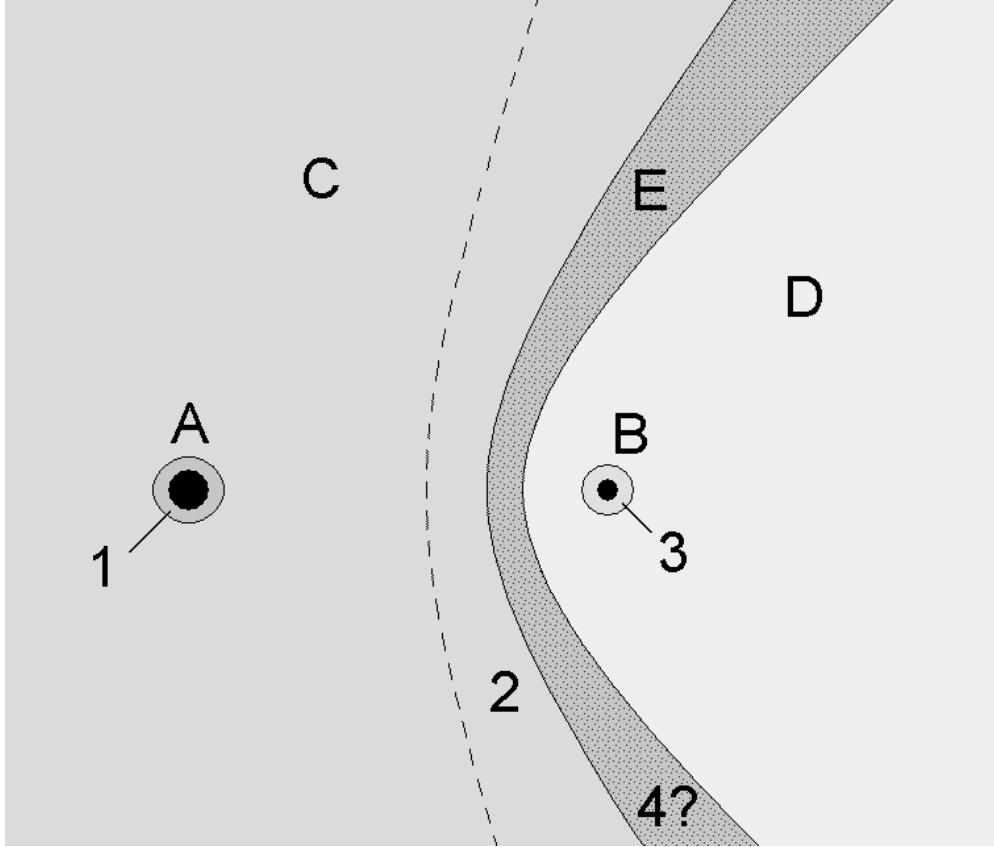


Fig. 12.— Schematic arrangement of distinct zones in a colliding-wind model with a hot secondary star. **A** and **B**: The two stars. **C**: The dense primary wind. **D**: The faster, less dense secondary wind. **E**: Hot shocked gas. **1**: The inner wind of the primary star may produce He I emission lines. **2** He^+ zone in the primary wind, photoionized by the secondary star. **3** Acceleration zone of the secondary wind, see text. **4** Small, dense cooled structures might exist within the shocked region, see text.

Table A1. The Harvard Objective Prism Plates of Eta Car

Plate Number	Calendar Date	Julian Date	Exposure Time minutes	Phase	Comment
X4005	5-15-1892	2412234	126	.94	missing
X4044	5-20-1892	2412239	60	.94	very weak exposure ^a
X4709 ^b	6-2-1893	2412617	37	.13	see text
X4725	6-6-1893	2412621	77	.13	narrow, underexposed
X4801	6-17-1893	2412632	70	.13	weak, on plate edge
X4846	6-23-1893	2412638	60	.14	weak, on plate edge
X4868	6-26-1893	2412641	–	.14	poor plate, all underexposed
X4869 ^b	6-26-1893	2412641	60	.14	weak exposure ^a
X5568 ^b	6-8-1894	2412988	60	.31	weaker than X4869 ^c
X6358	4-17-1895	2413299	–	.47	underexposed
X6480 ^b	5-2-1895	2413314	60	.48	no P Cyg profiles on emission lines ^d
X6592 ^b	5-25-1895	2413337	64	.49	no absorption lines, H and Fe emission
X7415	4-8-1896	2413658	60	.64	η Car not visible, but should be there!
A2224	3-12-1897	2413997	77	.81	H β emission
B19639	6-29-1897	2414106	121	.87	low dispersion, H β emission
B21154	4-11-1898	2414392	107	.01	low dispersion, H β emission
B21379	5-12-1898	2414423	158	.02	low dispersion, H β emission
A5787	4-8-1902	2415849	60	.73	looks like all later spectra ^e
X10482 ^b	6-5-1902	2415906	60	.76	–
X10494	6-7-1902	2415908	58	.76	–
X10505	6-10-1902	2415911	60	.76	–
X10513 ^b	6-11-1902	2415912	48	.76	–
X10644	1-16-1903	2416131	63	.87	plate missing
X10649	1-17-1903	2416132	64	.87	plate broken
X10658	1-20-1903	2416135	57	.87	plate missing
X10667 ^b	2-3-1903	2416149	60	.88	–
X10703	5-13-1903	2416248	91	.93	blurred
X10705	5-14-1903	2416249	63	.93	bad focus, plate broken
X10713	5-15-1903	2416250	62	.93	poor guiding
X10722 ^b	6-12-1903	2416278	65	.94	–
X10855 ^b	6-12-1904	2416644	53	.12	–
X12999	5-23-1913	2419901	112	.74	–
X13003	6-5-1913	2419914	87	.74	missing
X13009	6-30-1913	2419939	–	.75	weak exposure, η Car not visible
X13033	5-25-1914	2420278	60	.92	–
X13034	5-25-1914	2420278	60	.92	–
X13035	5-26-1914	2420279	60	.92	–
X13059	6-3-1916	2421018	62	.28	η Car not on plate
X13062 ^b	6-7-1916	2421022	97	.28	–
X13066	6-8-1916	2421023	90	.28	–
X13070	6-19-1916	2421034	101	.28	η Car not on plate
X13072 ^b	6-20-1916	2421035	83	.29	–
X13358	5-5-1922	2423180	60	.35	–
X13365	5-10-1922	2423185	61	.36	–

Table A1—Continued

Plate Number	Calendar Date	Julian Date	Exposure Time minutes	Phase	Comment
X13370	5-15-1922	2423190	56	.36	unwidened
X13371 ^b	5-15-1922	2423190	60	.36	–
X13373	5-16-1922	2423191	60	.36	–
X13376	5-17-1922	2423192	64	.36	–
X13396	6-1-1922	2423209	60	.36	–
X13408 ^b	6-12-1922	2423218	60	.37	–
X13410	6-13-1922	2423219	60	.37	–
X13412	6-14-1922	2423220	70	.37	missing
X13413 ^b	6-15-1922	2423221	64	.37	–
X13692 ^b	4-16-1923	2423526	57	.52	–
X13739	5-10-1923	2423550	85	.54	missing
X14861	5-3-1926	2424639	50	.07	–
X14939	6-15-1926	2424682	20	.09	–
X14961 ^b	7-1-1926	2424698	40	.10	–
X16486	3-11-1937	2428604	120	.03	missing?
X16492 ^b	5-2-1937	2428656	45	.06	–
X16493	5-2-1937	2428656	20	.06	poor spectrum
X16499 ^b	5-28-1937	2428682	45	.07	–
X16502 ^b	5-31-1937	2428685	120	.07	–
X16503 ^b	5-31-1937	2428685	49	.07	–
X16506	6-6-1937	2428691	120	.07	–
X16507	6-6-1937	2428691	45	.07	–
X16511	6-7-1937	2428692	120	.07	–
X16512	6-7-1937	2428692	45	.07	–
X16516	6-10-1937	2428692	120	.08	–
X16517	6-10-1937	2428692	45	.08	–
X16521	6-11-1937	2428696	20	.08	–
X16531	6-29-1937	2428714	20	.09	poor spectrum
X16602	3-20-1938	2428978	45	.22	rejected plate
X16605	3-21-1938	2428979	120	.22	poor spectrum
X16610	3-27-1938	2428985	70	.22	missing
X16614 ^b	3-29-1938	2428987	55	.22	good spectrum
X16618 ^b	4-10-1938	2428999	40	.23	–
X16664	1-2-1939	2429266	45	.36	missing
X16676	2-24-1939	2429319	120	.38	rejected plate
X16677	2-24-1939	2429319	20	.38	–
X16684	2-27-1939	2429322	4	.38	rejected plate
X16685	2-27-1939	2429322	45	.38	–
X16686 ^b	2-27-1939	2429322	20	.39	–
X16694	3-12-1939	2429335	45	.39	fuzzy image
X16695	3-12-1939	2429335	20	.39	–
X16698	3-16-1939	2429339	20	.39	–
X16701	3-17-1939	2429340	120	.39	–
X16704	3-19-1939	2429342	45	.39	–

Table A1—Continued

Plate Number	Calendar Date	Julian Date	Exposure Time minutes	Phase	Comment
X16707	3-20-1939	2429343	47	.39	–
X16708	3-24-1939	2429347	105	.39	η Car not on plate
X16710	3-26-1939	2429349	120	.39	–
X16715 ^b	4-10-1939	2429364	45	.40	–
X16720	4-16-1939	2429370	120	.40	–
X16724	4-19-1939	2429373	120	.41	–
X16729	4-20-1939	2429374	45	.41	–
X17165 ^b	5-1-1940	2429751	120	.60	–
X17170	5-6-1940	2429756	120	.60	–
X17174	5-7-1940	2429757	120	.60	fuzzy image
X17180	5-10-1940	2429760	120	.60	–
X17421	2-23-1941	2430049	120	.75	–
X17433	4-15-1941	2430100	45	.75	–
X17437 ^b	4-21-1941	2430106	120	.77	–
X17440 ^b	4-24-1941	2430109	45	.77	–
X17444	5-1-1941	2430116	120	.78	–
X17465 ^b	5-21-1941	2430136	120	.79	–
X17466	5-21-1941	2430136	35	.79	–
X17472	5-23-1941	2430138	120	.79	–
X17473	5-23-1941	2430138	45	.79	–
X17476	5-25-1941	2430140	120	.79	–
X17477	5-25-1941	2430140	45	.79	–
X17481	5-26-1941	2430141	120	.79	–
X17482 ^b	5-26-1941	2430141	45	.79	–

^aweak absorption line spectrum; $H\beta$, $H\gamma$, $H\delta$, [Fe II] 4359Å emission lines.

^bdigitized

^cabsorption lines barely discernible; $H\beta$, $H\gamma$ emission

^dabsorption lines very weak or gone; $H\beta$, $H\gamma$, $H\delta$, [Fe II] 4359Å emission.

^eHydrogen, Fe II, [Fe II] emission